Title

Emergent feed-forward and isohydric responses to drought stress and atmospheric aridity: Insights and physical intuition from a time-dependent soil and plant hydraulic model.

Author list

Fulton E. Rockwell

Affiliations

Corresponding author and email

Fulton E. Rockwell, fulton.rockwell@gmail.com

Orcids: 0000-0002-2527-6033

Summary

Drought and heat waves have synergistic effects on mortality as plants experience both supply and demand-side water stress. Yet which of these stresses most strongly down-regulates stomatal conductance (g_s), and whether patterns of regulation represent biological strategies or are imposed on the plant, remain at issue.

- Dynamic losses of soil hydraulic conductivity are modeled in a soil domain fed by a steady maximum water flux from a deep-water source. A root-uptake plane extracts water from the soil in a two-node (root and leaf) plant model, with g_s a function of leaf water potential.

- Multi-day simulations of a drought and heat wave experiment reproduce observations of anisohydric to isohydric transitions, driven by the balance of soil supply and atmospheric demand β. Feedforward control of transpiration E emerges from steep declines in soil hydraulic diffusivity that confine diurnal variation in moisture gradients and water discharge/recharge cycles to a shallow region at the root plane that thins in response to β.

- Empirical models of *VPD* sensitivity are compared to the full model to provide mechanistic insight into empirical model parameters. Apparent responses of g_s to *VPD* emerge from plant, soil and atmospheric feedbacks that are both time and scale dependent.

Keywords [plant drought response, vapor pressure deficit, soil hydraulics, heatwave, hydraulic limitation, stomatal conductance]

Table of word counts each section (I, MD, R, D). Num figs. Num Tables, num SI.

Total word count	10568	No. of Figures	8
Introduction	2629	No. of Tables	0
Model Description	2408	No. of Supporting Information files	6
Results	3122		
Discussion	2409		

Introduction

The dual role of stomata in admitting an inward flux of CO_2 while preventing the desiccation of vascular plant tissues has been recognized at least since Van Den Honert (1948), who proposed that stomata serve as the dominant resistance to water transport in the soil-plant-atmosphere continuum (‘SPAC’; Philip, 1966). While guard cells, as hydraulicly actuated valves, respond ‘passively’ to local water status, pore aperture is also decoupled from the local water potential of the epidermis by ‘active’ biochemistry (e.g., light activated ion pumping, ABA induced closure; McAdam & Brodribb, 2016; Jezek & Blatt, 2017), with the resulting complexity and interacting layers of regulation obscuring the control points that sense water status and ultimately govern stomatal behavior (Tardieu & Simonneau, 1998; Buckley, 2005; McAdam & Brodribb, 2016; Novick *et al.*, 2019; Jezek *et al.*, 2019; Grossiord *et al.*, 2020; Wankmüller & Carminati, 2022). While the twin stressors of heat and drought are known to have synergistic mortality effects (Mitchell *et al*., 2014; Matusick *et al*., 2018), the lack of a clear mechanistic description of how stomata integrate supply and demand stresses has led to controversy regarding plant responses to future climates, a debate focused on whether stomatal conductance is more limited by available soil water or atmospheric aridity (Roderick *et al.*, 2015; Novick *et al.*, 2016a, 2024; Berg & Sheffield, 2018; Grossiord *et al.*, 2020; Liu *et al.*, 2020a; McColl & Tang, 2024).

At the same time, the ‘active’ nature of stomatal regulation suggests that the 60% of global terrestrial evapotranspiration mediated by plant canopies is subject to a diversity of stomatal control strategies varying across species, functional groups and biomes (Tardieu & Simonneau,

1998; Oren *et al.*, 1999; Martinez-Vilalta & Garcia-Forner, 2017; Novick *et al.*, 2019; Wu *et al.*, 2021). Yet, transpiration can also be viewed as a ‘passive’ process in which water moves along gradients of its thermodynamic potential. Caught between Equivalent Water Thicknesses (EWT) for both the unsaturated soil zone and atmosphere on the order of centimeters, the plant canopy with an EWT on the order of millimeters may have little scope to express independent control of its water status at equilibrium (Shiklomanov, 1993; Hunt, Jr. *et al.*, 2009). In this perspective, the behavior of the plant canopy might be expected to follow that of any 'passive' material that, like soil, loses conductivity as it dries (Hochberg *et al.*, 2018; Feng *et al.*, 2019; Vargas Zeppetello *et al.*, 2023). With respect to the global water cycle, the plant canopy may approximate ‘green dirt.’

Physiologically, interest in vapor pressure deficit (*VPD*) responses as distinct from source water limitations began with evidence of ‘feed-forward’ stomatal behavior: stomatal closure that does not simply reduce increases in transpiration *E* with increases in atmospheric demand, but results in *lower E* (Franks *et al.*, 1997). Such behavior cannot be explained by the effect of simple steady-state feed-backs of *E* on guard cell water potential and stomatal apertures. Such feed-backs describe an incremental draw-down in water potential resulting from an incremental *increase* in *E*, thereby reducing the realized increase in *E*; yet, this form of regulation cannot reduce *E* itself (Cowan & Troughton, 1971; Franks *et al.*, 1997; Buckley, 2005). The inadequacy of simple hydraulic feedbacks, together with demonstrations at the physiological scale that leaf water potential and stomatal conductance do not follow a one-to-one relationship, has turned attention away from hydraulic control toward metabolic and chemical controls on stomatal responses to water stress (Turner *et al.*, 1984, 1985; Gollan *et al.*, 1985; Simonneau & Tardieu, 1998; McAdam & Brodribb, 2016).

Fundamentally, this change of research focus makes sense: the principal activity of guard cell physiology is to break any one-to-one relationship of pore aperture to water potential by manipulating ion concentrations (and so osmotic potential and turgor) in response to a complex array of signals and forcings, including ABA, photon flux density and light quality, diurnal patterns in substrate availability and enzyme activation, CO_2 concentrations and temperature (Schroeder *et al.*, 2001; Messinger *et al.*, 2006; Brodribb & McAdam, 2011; Buckley, 2019; Jezek *et al.*, 2019). Despite, or perhaps because of the richness of physiological detail that has been described at the guard cell level, efforts to predict whole plant responses to environmental

forcing at scale have embraced empirical approaches that produce behavior consistent with physiological response patterns but do not require mechanistic closure (Anderegg *et al.*, 2017; Mrad *et al.*, 2019; Grossiord *et al.*, 2020; Wang *et al.*, 2020; Mencuccini *et al.*, 2024).

The most widely adopted empirical approach to partitioning changes in stomatal aperture between supply and demand limitation has been to model maximum stomatal conductance ($g_{s,\mathrm{ref}}$) as a function of soil moisture, and then fit a slope parameter (m) that describes the erosion of conductance with increasing vapor pressure deficit (*VPD*) (Oren *et al.*, 1999; Novick *et al.*, 2016a, 2019; Grossiord *et al.*, 2020). Adopting this approach, Novick et al. (2016a) fit flux tower data to predict the response of canopy conductance to expected future increases in *VPD* with climate warming. This approach has attracted the criticism that soil moisture and *VPD* are not independent at the spatial and temporal scales relevant to climate (Roderick *et al.*, 2015; Novick *et al.*, 2016a; Berg & Sheffield, 2018; Liu *et al.*, 2020a). Even at the sub-daily physiological scale of flux tower data over which bulk soil moisture and *VPD* are more weakly correlated (Novick *et al.*, 2024) it is unclear to what extent apparent stomatal responses to *VPD* are truly independent of soil moisture stress, or driven by dynamic losses in soil conductivity that are poorly captured by bulk soil moisture measurement (Novick *et al.*, 2019; Koehler *et al.*, 2024), and whether parameterizing independent soil and *VPD* responses amounts to double counting (Liu *et al.*, 2020b).

At daily time scales, an empirical approach has been developed that predicts E and surface conductance solely from weather data. The ETRHEQ hypothesis (EvapoTranspiration from Relative Humidity at Equilibrium) minimizes the vertical variance of RH through the Atmospheric Boundary Layer (ABL) to find the surface conductance (interpreted as g_s; Grossiord *et al.*, 2020), and so can be used to construct a response of g_s to *VPD* (Salvucci & Gentine, 2013; Rigden & Salvucci, 2015).

As an empirical steady-state theory, ETRHEQ does not specify the mechanisms driving the relationships it describes. To address this gap, McColl *et al*. (2019) and McColl & Rigden (2020) provided a simple theory of Surface Flux Equilibrium (SFE) that relates the RH of the ABL to the balance of latent and sensible heat at the surface. As the system evolves toward an ‘equilibrium’ steady-state at which inputs from the surface match the fluxes out of the top of the ABL, the state of the land surface becomes fully reflected in the state of the atmosphere, over

time scales ranging from daily for ‘wet’ surfaces, to somewhat longer for ‘dry’ surfaces (McColl & Rigden, 2020).

As SFE is an ‘equilibrium’ theory, the direction of causality between variables such as RH and g_s cannot be inferred based solely on their internal relationships in the stationary-state. Nor does SFE necessarily offer a unique explanation for ETRHEQ. What SFE does do is capture the ansatz described by ETRHEQ in a model that includes feedbacks on *E* due to humidification and heating of the atmosphere by the surface heat and moisture fluxes, but not a prescribed biological response of g_s to *VPD*. This result raises the question of whether the surface conductance g_s at this scale is primarily physically constrained, or determined by active biological optimization or adaptive strategies for stress avoidance (Konings & Gentine, 2017; Wu *et al.*, 2021; Vargas Zeppetello *et al.*, 2023; Mencuccini *et al.*, 2024).

One thing often missing in the current debate is an appropriate ‘null model’ for environmental control (e.g., Hochberg *et al.*, 2018; Vargas Zeppetello *et al.*, 2023) that might be employed to identify biologically versus purely physical regulation of *E*. Such a model might address to what extent the parameters in empirical models of stomatal *VPD* sensitivity represent physical feedbacks on stomatal conductance from soil or plant xylem, or autonomous stomatal behavior, a gap in understanding that has led to calls for further work on the problem (Novick et al., 2019; Grossiord et al., 2020). In addition, there appears to be continued confusion regarding whether the isohydric-anisohydric spectrum of behavior (as variously defined) describes a biologically controlled adaptive water management strategy, or simply reflects physical limits imposed on the plant by soil and atmospheric aridity (Konings & Gentine, 2017; Martínez-Vilalta & Garcia-Forner, 2017; Hochberg *et al.*, 2018; Feng *et al.*, 2019; Novick *et al.*, 2019; Wu *et al.*, 2021; Mencuccini *et al.*, 2024).

As a step toward such a physical null model, this study develops a time-dependent SPAC model from a continuum approach to soil water transport coupled to an ohmic (discrete) plant with stomatal conductance responding solely to leaf water potential. The goal is not to build an exhaustive mechanistic model of the SPAC (Tuzet *et al.*, 2003), nor to provide a sub-model appropriate for incorporation into large-scale land surface and atmosphere models (Sloan *et al.*, 2021). Rather the aim is to construct a minimal hydraulic representation of the SPAC for understanding physical and environmental contributions to experimentally observed patterns of

transpiration (Drake *et al.*, 2018). Demonstration of the competence of a hydromechanical null model could help identify the physical factors contributing to the fitted parameters in more scalable empirical models of stomatal responses to *VPD* and soil drought (Attia *et al.*, 2015; Konings & Gentine, 2017; Novick *et al.*, 2019; Mrad *et al.*, 2019; Grossiord *et al.*, 2020; Mencuccini *et al.*, 2024).

Stomata are undeniable biological, and yet their importance as a controlling resistance in the SPAC makes their inclusion in even a minimal 'physical' model essential (Van Den Honert 1948; Jarvis & McNaughton 1986). In doing so, a distinction between 'passive' or 'physical' stomatal responses and 'active' biological responses can be drawn. Over long (non-physiological) time scales, the average water potential-stomatal conductance relationship generally follows a monotonic decline of g_s in response to water stress (Brodribb & Holbrook 2003; Anderegg *et al.*, 2017; Levin *et al.*, 2019). Stomatal closure in this case may be regarded as thermodynamically 'passive' in the sense that the response does not require the plant to do further work. With this framing, examples of ‘active' or 'biological responses’ include changes in the stomatal response curve to local water potential by osmotic adjustment (*e.g.*, a shift in the water potential for 50% closure $g_s\Psi 50$), or deviations from the curve to satisfy a biological constraint (*e.g.*, conservation of water use efficiency, internal CO_2 concentration). The 'active' vs 'passive' distinction here does not follow the definition of Brodribb & McAdam (2011), centered on ABA responses, but is meant to distinguish between stomatal behaviors that can be adequately captured by a single integrative variable - local water potential - versus behaviors requiring additional parameterizations. A 'minimal hydraulic model' then is one that assembles a set of functions that are all passively driven by water potential.

The interplay of supply and demand functions in limiting transpiration

Dynamic losses of conductivity somewhere along the SPAC have the potential to amplify stomatal sensitivity to *VPD* by increasing the hydraulic feedback of transpiration on the leaf water potentials constraining stomatal conductance. The general behavior emerging from dynamic losses of conductivity – conductivity that declines as the local potential becomes more negative – is for the flux to approach a maximum in the limit of an infinite driving force. Two principle sites for such dynamic losses have been proposed: within stem xylem (Sperry & Love, 2015), or in the soil proximal to the root (i.e., rhizosphere; Cowan, 1965; Carminati & Javaux,

2020). A third possibility is that dynamic losses of conductivity could arise within leaves through minor vein collapse, or across the membranes of bundle sheath or mesophyll cells (i.e., outside xylem; Shatil-Cohen *et al.*, 2011; Zhang *et al.*, 2016; Scoffoni *et al.*, 2017; Jain *et al.*, 2024a,b). This last case is not explored further here as the expected impact of a variable leaf resistance at the whole plant scale generally follows that of the xylem case (albeit with differences in time scales of recovery), which can then be thought of as representative of the general case of a variable conductance occurring within the plant.

Sperry *et al.* (1998) modeled water transport through a discretized soil-plant continuum, accounting for stress induced declines in both soil hydraulic conductivity and plant xylem conductivity, concluding that xylem vulnerability was likely to be the dominant dynamic factor contributing to stomatal regulation. Carminati & Javaux (2020) took a similar approach to Sperry & Love (2015), finding that with their parameterization soil conductivity emerged as the factor limiting transpiration. In addition to losses of hydraulic conductivity in the soil itself, root-soil contact has emerged as another source of variable resistance that might explain apparent soil resistances that exceed the level predicted by root density and soil properties (Herkelrath *et al.*, 1977). Drying of root mucilage or root shrinkage with the onset of soil water stress could lead to an increase in air gaps between the soil and roots (McCully et al., 1997), with liquid flow across the contact zone increasingly replaced by relatively inefficient water vapor diffusion, creating a bottle neck (Carminati *et al.*, 2009, 2016; Rodriguez-Dominguez & Brodribb, 2020; Manandhar *et al.*, 2024; Akale *et al.*, 2025).

Cowan (1965) modeled time-dependent behavior of E in drying finite volumes of soils (pots) to show that dynamic declines in soil water content and hydraulic conductivity proximal to the root could constrain E during the day, followed by recovery overnight, even as bulk soil moisture declined monotonically over multiple days (Fig. 11 in Cowan, 1965). Stomatal conductance was not explicitly modeled, so the relationship between dynamic conductivity and realized stomatal behavior remained unexplored. Instead, in these and similar studies of soil influences on stomatal regulation, a critical leaf water potential for stomatal closure was defined that effectively served as a transition point from perfect anisohydry to perfect isohydry (Cowan, 1965; Hochberg *et al.*, 2018; Javaux & Carminati, 2021). This simplification is helpful as introducing a stomatal

conductance that both determines and responds to transpiration through a dependence on leaf water potential complicates solution.

Tuzet *et al.* (2003) constructed the most complete model of the SPAC to date, as far as the author is aware. This model follows Cowan (1965) in modeling time dependent soil moisture in a cylinder of soil around a representative root within a finite soil volume, but adds g_s as a logistic function of leaf water potential with additional forcing from internal CO_2 concentrations and a photosynthesis model, driven by diurnally varying radiation and surface energy balance with a boundary layer. This model generated both isohydric and anisohydric behavior, and feed-forward stomatal closure that was suggested to be driven by the soil. However, the complexity of the model prevented fully accounting for the generated behavior. A further weakness acknowledged in Tuzet *et al.* (2003) was that they were unable to locate a suitable data set whose behavior they could attempt to reproduce and explain.

Here a heat wave experiment (Drake *et al.*, 2018) using whole tree gas exchange chambers is modeled to test whether a minimal hydraulic time-dependent approach can successfully recover observations of: 1) intra-day feed-forward stomatal behavior in response to diurnally varying *VPD*, 2) conservation of total daily transpiration across days and *VPD* levels, and 3) isohydric responses to *VPD* forcing across treatments. The model of the heat wave experiment is then employed to explore the effectiveness of a counter-factual (unobserved) osmotic adjustment to maintain carbon gain. Finally, two empirical steady-state models are compared for their ability to capture patterns of stomatal sensitivity to *VPD* that emerge over physiological (hourly to diurnal) versus diel (24 hour to multi-day) time scales, and these are then compared to the patterns of *VPD* and g_s expected under SFE at the flux tower scale.

Model Description

Model structure and analysis of basic behavior

In the Drake *et al.* (2018) experiment, eucalyptus trees (~ 6 m tall) were individually enclosed in 9 m tall chambers that allowed control of temperature and humidity as well as measurements of gas exchange (CO_2, H_2O). The goal of the experiment was to understand the physiological impact and response of pre-droughted trees to a heat wave ('Heat Wave' treatment), combining air temperature (daily peak 43-44°C) and *VPD* stress (daily peak 5-6 kPa), versus a Control

subject to typical atmospheric conditions (daily peaks of 28-29 ^{o}C, 2-2.5 kPa). Figure 2 in Drake *et al.*, (2018) shows that the trees subject to the Heat Wave treatment showed no increase of total daily transpiration over the control despite a doubling of *VPD*.

In this experiment, irrigation was withheld from the enclosed plants in both treatments, leaving ground water as the only possible source for recharging a diurnally drying soil domain. Incorporating a ground water source into the time-dependent model framework of Cowan (1965) or steady-state analysis of Carminati & Javaux (2020) would be impractical due to a mismatch in scale and geometry. In those models, the steepest gradients in soil water content and potential are expected to occur over a centimeter to millimeter scale in a cylindrical domain around an individual root, yet transport from the water table is most readily described using a one-dimensional cartesian frame over a scale of centimeters to meters.

To resolve such mismatches of geometry and scale, a flux boundary condition is proposed based on an asymptotic maximum soil flux that emerges from the soil hydraulic vulnerability function and the distance from a water source to the root zone. (Gardner, 1958; Gardner & Fireman, 1958; Jury *et al*., 1991; Supplemental Information Notes S1). Physically, as the maximum flux is approached, water columns in the soil break as they are pulled harder resulting in vanishingly small increases in flow rate (Supplemental Information Figure **S2**). While in the limit of infinite dryness the uncoupling of matric potential and soil flux may appear non-physical, it results from the same mechanics in Sperry & Love (2015), Cowan (1965) and Carminati & Javaux (2020): in all three cases as E approaches a maximum, the driving potential (e.g., leaf water potential or soil matric potential near the root) diverges, such that further increases in the driving force increase the flux infinitesimally due to concurrent reductions in conductivity.

To maintain the one-dimensionality of the model space, root uptake is further abstracted (Fig. **1**). The cylindrical geometry of the soil domain around an individual root (Cowan, 1965; Sperry *et al*., 1998; Carminati & Javaux, 2020) is replaced by an ‘uptake plane’ introduced at an effective or characteristic rooting depth for the system (Binks *et al*., 2022). Though it may seem artificial relative to a rooting volume, the concept of a rooting plane captures the behavior of uptake being dominated by the roots in contact with the wettest soil region, independent of the vertical distribution of rooting density (Dawson *et al.*, 2020). It is also consistent with the one-dimensional representation of the plant canopy in SPAC models (Philip 1966). Nevertheless, this

abstraction comes at the cost of not capturing the extra ‘geometrical resistance’ created by the concentration of the flux as it approaches the root in a cylindrical domain (Cowan, 1965). Representing the root zone as a ‘plane of uptake’ then rests on the hypothesis that geometrical amplification of soil resistance is not essential for capturing the behavior of the physical experiment.

The flux of water out of the soil domain is driven by transpiration from a discrete plant featuring two nodes (root and leaf water potential) separated by a constant whole plant conductance (Supplemental Information Notes **S1**). The neglect of cavitation in the plant is justified by leaf and stem measurements in the Supplemental Information of Drake *et al.* (2018) that show no reduction in hydraulic conductance occurred during the experiment. The neglect of plant capacitance follows Cowan’s (1965) arguments that soil capacitance is expected to dominate the time scale of storage effects.

As the trees in the physical experiment were in large chambers with well-stirred air, it is assumed that aerodynamic canopy conductance was non-limiting and so total canopy conductance was close to stomatal conductance, and leaf temperature close to air temperature (*e.g.*, Fig. 4 in Drake et al 2018). In this isothermal well-mixed limit, atmospheric humidity is 'imposed' at the leaf surface, and transpiration can be expressed as the product of stomatal conductance and *VPD* (Jarvis & McNaughton, 1986). To model the diurnally transient behavior in the Drake experiment, transpiration is represented as the product of a peak transpiration rate (E_p) that carries the units of cm day^{-1} with three dimensionless factors that introduce variations into *E*. The first is a diurnal demand function *f(t)* (Fig. **1b**) that produces a sinusoidal range from 0 to 1, representing the effects of both diurnal variations in air temperature on *VPD* and variations in stomatal aperture as light levels change over the day. The second is a non-dimensional nominal *VPD* level (*nVPD*, 1 to 2.5) that represents daily peak atmospheric sink strength, and the third is a non-dimensional stomatal conductance (0 to 1) that depends on leaf water potential and captures the effect of water stress on the realized evaporation rate (Fig. **1c**). In this framework, it is useful to distinguish between 'Potential transpiration' *PE*, which represents the transpiration rate that would be realized at maximum stomatal conductance, and the actual transpiration *E* inclusive of stomatal water limitation effects,

$$PE = E_p\, nVPD\, (1 - \cos 2\pi t/\tau_d), \qquad eq.1$$

$$E = E_p\, nVPD\, g_s(\Psi)\, (1 - \cos 2\pi t/\tau_d), \qquad eq.2$$

where τ_d is the period of diel oscillation of one day.

In the above model structure, the only possible source of a time-dependent variable liquid phase resistance that could impose water stress on the leaf, and so throttle stomatal conductance and E at sub-daily time scales, is in the 10 cm deep soil domain. In this region changes in water content, due to discharge by root uptake and recharge from the deep-water source, are related to changes in hydraulic conductivity and flux by Richard's equation (Fig. **1d**), neglecting gravitational effects over the 10 cm change in height. The governing equation, boundary conditions, and initial conditions are then linearized using the Kirchhoff transform, leading to the expression of soil water content θ, soil matric potential h, and leaf water potential Ψ in terms of a single variable φ, a potential flux with diffusive units of $cm^2\ day^{-1}$. Here we take the step of non-dimensionalizing φ and time t and length z, and re-scaling the governing equations and boundary conditions to express them as functions of the non-dimensional potential flux $\Phi = \varphi/(H\, J_m)$, time $T = t/\tau_d$, and length $Z = z/H$, where H is the height of the model domain. This approach organizes all the parameters in the model into a few non-dimensional groups that describe the behavior of the solution (Supplemental Information Notes **S1**):

$$\frac{\partial \Phi}{\partial T} = \frac{\tau_d}{\tau_D}\Phi\frac{\partial^2 \Phi}{\partial Z^2}, \quad \tau_d = 1, \quad \tau_D = \frac{H}{J_m D_o}. \qquad eq.3$$

$$-\frac{\partial \Phi}{\partial Z}\Big|_{Z=0} = 1. \qquad eq.4$$

$$-\frac{\partial \Phi}{\partial Z}\Big|_{Z=1} = \beta\, g_s(\Phi)\, (1 - \cos 2\pi T), \quad \beta = \frac{E_p\, nVPD}{2\, J_m}. \qquad eq.5$$

$$\Phi(0, Z) = \frac{1}{H\, J_m}. \qquad eq.6$$

The model takes the form of a non-linear diffusion equation, where the non-dimensionalized soil diffusivity, $D_o\Phi$, introduces non-linearity through its dependence on the potential flux itself (note that D_o is a pure number). Conceptually, the soil diffusivity represents a balance of soil hydraulic conductivity to soil hydraulic capacity (water storage).

There are two timescales in the problem, as can be seen in eq. 3. The first is the period of oscillations in potential transpiration of one day, τ_d, the diel time scale in eq. 2. The second is the diffusive timescale τ_D, the characteristic time for the soil domain to attain a new steady state after a perturbation at the boundary. The diffusive time τ_D is larger (slower) for larger domain sizes (the distance H) and smaller fluxes from the water table J_m. Larger values of D_o mean that conductance dominates soil capacitance contributing to faster response times (damping is low), while smaller values mean soil capacitance dominates conductance, slowing response times (damping is high). These two timescales appear in the model as a ratio, meaning that what will matter for model behavior is how quickly the soil domain can respond relative to the speed at which the conditions at the rooting plane change. However the time dependent behavior of the model is not entirely predictable from this ratio of time scales due to the non-linearity inherent in $D_o\Phi$. The effective diffusivity will deviate from the nominal value D_o with time and position in the soil domain, with important consequences for the behavior of the model.

As the long-term behavior of the model is expected to be independent of the initial condition (eq. 4), the only remaining parameter driving model behavior is β (eq. 5). β represents the balance of potential evaporation *PE* to the steady 'maximum flux' into the lower boundary of the domain. As the value of the time-varying term (eq. 5) integrated over a single day is 1, a β of 1 means that the total daily flux from the source into the soil domain (eq. 4, always equal to 1) balances total daily *PE* out of the domain, allowing normalized stomatal conductance to remain near its maximum value of 1. As *nVPD* exceeds 1, total daily *PE* exceeds the total daily water flux into the domain, causing Φ to fall in the soil domain and thereby forcing stomatal closure until average fluxes of water into and out of the soil domain come approximately into balance: there is nothing in the model that forces a balance of inputs and outputs at the daily scale, and longer oscillations in total daily E over days are possible, though expected to damp-out.

At sub-daily timescales, even at β =1 peak potential transpiration rate exceeds the steady flux into the soil domain by a factor of 2. However, due to soil capacitance and discharge of water as φ falls in the domain, stomatal closure need not occur over the course of the day. If the constant influx from the source is sufficient to fully re-charge the soil domain overnight, the cycle of daily peak E exceeding the steady inward flux can continue. For β >1, as the soil attempts to keep pace with potential transpiration stomatal regulation will at some point be triggered in a manner

sensitive to the scale in the imbalance of supply and demand and the ratio of atmospheric to soil timescales.

Parameterization for the heat wave experiment

The dimensional potential transpiration rate, E_p, was set to a rate of 0.3 cm day^{-1} to match the intraday peak of 2 mmol m^{-2} s^{-1} seen in the controls for the heatwave experiment (Drake *et al.*, 2018; Fig. 2c). Peak *VPD* for the control (~ 3 kPa) was set as the reference value for normalizing *VPD*. With these normalizations, stomatal (or canopy) conductance ranges from one to zero: E_p can also be interpreted as the dimensional peak stomatal conductance. The maximum flux from the water table J_m was then set to half of E_p, 0.15 cm day^{-1}. As the integral of the demand function over one day evaluates to 0.5, this choice of parameterization exactly balances the flux from the water table with total daily transpiration at a *nVPD* of 1 for the stress-free Control treatment (no stomatal limitation). For the Heat Wave treatment (*nVPD* 2), daily peak and total potential daily *E* were 0.6 cm day^{-1} and 0.3 cm day^{-1} respectively, double that of the Control.

Stomatal conductance is parameterized as a sigmoidal function of leaf water potential, a functional form motivated by both typical field observations (Anderegg *et al*., 2017; Levin *et al*., 2019) and direct hydromechanical experiments (Franks & Farquhar, 2007). The shape parameter controlling the steepness of the curve and the water potential for 50% stomatal closure ($g_s\Psi 50$) were fit together with total plant hydraulic conductance (K_{plant}) to reproduce the midday water potentials reported for the Heat Wave treatment in Drake *et al.*, (2018), while also producing a minimal stomatal response ('stress-free' condition) for the Control.

As the soil properties for the Heat Wave experiment were unavailable from Drake *et al.* (2018), the hydraulic conductivity and matric potential functions of water content were parameterized based on Cowan (1965) for Yolo light clay. With this parameterization, a maximum steady soil flux of 0.15 cm day^{-1} develops over a distance of 50 cm between a water source and rooting plane (Supplemental Information Figure **S3**), similar in magnitude to the one-meter distance between the depth of greatest change in soil water content (50 cm) and no change in soil water content (150 cm) given by neutron counts for the soils in Drake *et al.* (2018). By way of comparison, for the fine sandy loam (Pachappa) and clay (Chino) soils studied by Jury *et al.* (1991), a flux of 0.15 cm day^{-1} occurs over a distance of 130 and 155 cm respectively (Supplemental Information Fig. **S2**). These distances support a hypothesis that in the physical experiment soil properties and

distance from source to sink on the order of a meter could have imposed the observed daily maximum flux of 0.15 cm day^{-1}. Finally, to initialize the model soil water content in the model domain was set to a uniform value θ = 0.25 (*i.e.*, φ=1), about half field capacity (Philip, 1957).

Model runs

To generate a range of behavior in the model different values of β, the ratio of potential daily evaporation to total daily soil flux, were investigated. In a first pair of model runs, β=1 was specified for the Control, and β=2 for the Heat Wave. In a second pair, the Control was set to an incrementally more stressful level β=1.25, and again doubled for the Heat Wave to β=2.5. By construction, β is equivalent to *nVPD*, which also serves as a descriptor of atmospheric aridity across the different model runs. Both *nVPD* and β will be used here to emphasize respectively either the effect of variations in *nVPD* given a fixed daily integrated soil flux (as in the Drake experiment), or the general phenomena of a balance of supply and potential demand β seen by stomata.

The first three days of each model run represent a transient period during which the initial uniform soil moisture decays to a repetition of the same cycle each day, leaving a four-day period comparable to the Heat Wave experiment. This repeated daily cycle is referred to as a stationary-state. To test the effect of a reduction in the water potential for a 50% reduction in g_s (i.e., $g_s\Psi 50$), a proxy for leaf osmotic adjustment, two additional model runs were compared with $g_s\Psi 50$ set to -1.33 or -2.66 MPa, and β=1 or 2, with other parameters unchanged. The models and figures were coded and evaluated in Mathematica 14 (Wolfram Inc., Champaign IL, USA; Supplemental Information Notes **S4**).

Results

Heat Wave: Recovery of intra- and inter-day patterns of transpiration under a doubling of VPD

Following a three-day initialization period, the model reproduced diel stationary states and inter-day conservation of *E* across both treatments, as in the physical experiment of Drake *et al*. (2018; Fig. **2**). As inter-day and across-treatment conservation of *E* emerges from the model and is not directly imposed, other behaviors could be produced for some initial conditions, including negative values (foliar uptake: hydration of the soil from the atmosphere at the dew point, not observed by Drake *et al.* (2018)) or longer-phase (multi-day) oscillations of the potential flux

(data not shown). The model was judged to have converged on a solution when the total daily flux into the rooting plane reached a stable value of 0.15 +/- 0.005 (3.33%) cm day^{-1}. With respect to the physical Heat Wave treatment, the model reproduced a shift of peak *E* to earlier in the AM relative to the control, and a steep 'feed-forward' decline in *E* as *nVPD* increased to its diurnal peak (Fig. **2a)**. Rooting surface water potentials were sufficiently dry that no serious errors were introduced by assuming a steady maximum flux at the lower soil domain boundary (Fig. 2b, Supplemental Information Figure **S5**), and diurnal variations in φ, *h*, and Ψ did not reach the source side of the model domain from the rooting plane, indicating the 10 cm depth was sufficient to capture all time dependent soil effects (Supplementary Information Figure **S6**). Stomatal limitation in the Heat Wave treatment was 75% of the control, far less than the 50% reduction in assimilation seen in the physical experiment: the difference seems appears likely due to thermal inhibition of photosynthetic capacity (Drake et al., 2018).

For the 'stress-free' condition of an *nVPD* of 1 adopted for the control, diurnal drying of the soil and leaf (Fig. **2b**) produced only slight stomatal limitation of *E* at the midday peak (Fig. **1c**, blue), such that transpiration closely followed the diurnal variations in potential transpiration (Fig. **1a**, blue). Examination of the diurnal cycles of root and leaf water potentials (Fig. **2b**) shows how aggressively soil loss of conductivity depressed root and leaf water potential in the Heat Wave treatment, creating an anisohydric type stomatal response across *nVPD* levels (Martínez-Vilalta *et al.*, 2014), with midday leaf water potential falling to -1.5 MPa versus -0.6 MPa for the Control. This result did not match the pattern in the physical experiment, for which midday leaf water potentials between treatments remained near -1.5 MPa across treatments in an isohydric manner (Supplemental Information in Drake *et al.*, 2018).

Setting the *nVPD*s for the two treatments to the moderately more stressful levels of 1.25 and 2.5 maintained the previous pattern in the Control of *E* following the diurnal course of potential *E*, while again showing feed-forward declines in the Heat Wave (Fig. **3**). Yet, now midday minimum leaf water potentials of the Control approached closer to those in the Heat Wave (-1.2 vs -1.5 MPa; Fig. **3b**) than in the previous set of model runs (Fig. **2b**), marking a shift in the response of leaf water potential to the doubling of *nVPD* from anisohydric to isohydric. This shift in behavior derived from root surface drying at 1.25 *nVPD* pushing leaf water potential

more negative than -1 MPa, such that the stomatal conductance entered the region of steep declines centered on $g_s\Psi 50$, resulting in stricter (more isohydric) regulation of E (Fig. **1c**).

The above result suggests that both the location of $g_s\Psi 50$ and the degree of soil drying (induced by an increase in *VPD*) control the transition from anisohydric to isohydric behavior. Yet, running the model for both *nVPD* 1 and 2 with $g_s\Psi 50$ doubled from -1.33 to -2.66 MPa (Fig. **4**) shows that once the gradient at the rooting plane begins to steepen in response to elevated *nVPD* (Fig. **4e** vs **4b**), the water potential at the rooting surface drops precipitously to force leaf water potential to whatever level is required to limit transpiration to the available soil flux (Fig. **4f** vs **4c**). The ultimate effect of 'osmotic adjustment' in the stomatal setpoint $g_s\Psi 50$ was then simply to steepen the peak and resulting feedforward behavior of the Heat Wave trees (Fig **4a** vs **4d**) and to lower the minimum leaf water potential (Fig. **4c** vs **4f**) but without extracting any more water out of the soil over the course of a day.

General controls on the emergence of feed-forward and isohydric behavior

That the shift in the treatment pairings of *nVPD* from 1 and 2 to 1.25 and 2.5 saw a shift from anisohydric to isohydric patterns in leaf water potential without the emergence of strong feed-forward declines in E at *nVPD* 1.25 suggests these behaviors may be independent. Sensitivity analyses show that this apparent independence is true only in part (Fig. **5a**). Varying β from 1 to 5 in the base model (with nominal diffusivity D_o=25.7) shows that feedforward behavior steepens as the imbalance of supply and demand become large (Fig. **5a**), while isohydry emerges rapidly between β 1 and 2, with only a small further decline in midday leaf water potential as the imbalance grows to β=5 (Fig. **5b**). Both the emergence of feedforward and isohydry can result from increasing β. Yet, this coupled response is not seen for low values of the soil diffusivity, as might occur for soils with higher clay fractions (lower conductivity and higher capacitance than sand; Jury *et al.*, 1991; Koehler *et al.*, 2024; Wankmüller *et al.*, 2024)).

Lowering the nominal diffusivity in steps from 25.7 to 1 while holding β at 2.5 shows that feedforward behavior vanishes as the time scales for the soil to respond to diurnal changes in demand become longer, effectively smoothing E over the course of the day (Fig. **5c**). This change in feedforward behavior across levels of soil diffusivity is unaccompanied by any significant change in the behavior of midday leaf water potentials (Fig. **5d**), such that the degree of isohydry is less sensitive to the soil diffusivity than feedforward behavior. This difference in

sensitivity is confirmed by a sweep of β from 1 to 2.5 at D_o=1 (Fig. **5e,f**). In this 'slow' soil regime, peak broadening, without an a.m. spike that turns into decay, replaces feedforward behavior as β becomes large (Fig. **5e**), while midday leaf water potentials show the same transition to isohydry as for high D_o (Fig. **5f**). Isohydry develops due to the supply imbalance β >1 alone, with the particular midday water potential the leaf is pushed to set by $g_s\Psi 50$ (Fig, 4 **c,f**).

Examining the spread between the gradients of water potential in the soil domain at the minima and maxima of the diel cycle of *nVPD* shows how low soil diffusivity suppresses the development of feedforward behavior in response to β >1 (Fig. **6**). At a stress free β=1, E tracks potential E at both low (D_o=1; Fig. **6a**) and high (D_o=25.7; Fig. **6b**) nominal soil diffusivities, with only a slight lag at the lower value. Yet despite similar behavior in E the gradients in the soil behave very differently. At the lower diffusivity, the soil is slow to respond to the diel cycle such that capacitive discharge is damped and overnight relaxation is small (Fig. **6c**). At the higher nominal diffusivity, the time scale for the soil to respond to changes in demand at the rooting plane is fast relative to the period of oscillation, and so the soil gradient relaxes overnight to a large degree (Fig. **6e**). This difference in the behavior of the gradients follows the 'damping depth,' δ, the distance from the rooting plane into the soil domain that diel oscillations are expected to reach:

$$\delta = \sqrt{\frac{2\, D_o \varphi}{\tau_d}}, \qquad eq.7$$

At the low nominal diffusivity, the soil gradient oscillates only within the last cm at both β=1 and 2. The time invariant part of the gradient from z=0 to z=9+ cm carries the steady flux of 0.15 cm day^{-1} with no capacitive discharge (Fig. **6c,d**), while the midday excess transient flux up to the peak of 0.3 cm day^{-1} is met by capacitive discharge within the last cm before the rooting plane. As the gradient hardly relaxes, when β is doubled to 2 it is already diverging and the flux becoming asymptotic (compare Fig. **6c** to **6d)**, with the result that stomata are rapidly pushed toward their $g_s\Psi 50$ and E fails to follow potential E above the steady state flux (Fig. **6a**, dashed red vs solid red lines).

For both fast and slow soils, the doubling of atmospheric demand relative to the steady inward soil flux from the source J_m spreads the net discharge of stored water over a longer period that

starts earlier in the day. This leaves less dischargeable water to meet peak midday demand, leading to a collapse in midday E relative to β=1 (Fig. **6a**) for both high and low nominal diffusivity. Yet, the difference in nominal diffusivities leads to an important difference in the diurnal distribution of discharged water, a difference that drives the emergence of a feedforward pattern. At high nominal diffusivity, relaxation of the soil gradient is pronounced, with the damping depth extending below 9 cm (Fig. **6b,e**). When potential E is doubled at $nVPD$ 2, the increased relaxation (relative to low diffusivity) allows capacitive discharge to be 'pulled-forward' in the early a.m. (skewed light blue area in Fig. **6b**) before the soil gradient diverges and pushes the stomata to their $g_s\Psi$50 (Fig. **6f**). This greater supply-elasticity in discharge for a 'fast' soil allows E to track potential E for longer and to a higher rate in the a.m. than at low soil diffusivity, though ultimately at the cost of p.m. E. This early peak then collapses in a feedforward manner as the soil gradient diverges and soil capacitive water release becomes exhausted, requiring that the asymptotic level of E decay toward the steady flux (Fig. **6b**, red dashed vs red solid lines).

A further important factor contributing to feedforward behavior is the degree of confinement of capacitive water release (shallowness of the damping depth) that occurs in the soil domain. As discussed, at β=2 a higher nominal diffusivity leads to a deeper damping depth and greater overnight gradient relaxation (Fig. **6d,f**) that allows E to track potential E farther along its curve (Fig. **6a,b**), yet it is also important for feedforward collapse that, at constant nominal diffusivity, as β is doubled the damping depth drops by more than half (Fig. **6d** vs **6c**, **6f** vs **6e**). This decrease occurs due to the non-linearity inherent in the realized diffusivity's ($D_o\varphi$) dependence on the local moisture state of the soil. Evaluating δ (eq. 7) at the rooting plane (z=10) selects the lowest value of the soil diffusivity $D_o\varphi$ in the system, and it is this minimum diffusivity that appears to control the observed damping depths (Fig. **6c,d,e,f**). As β increases both in the a.m. and across treatments, $D_o\varphi$ at the rooting plane decreases, and this shallowing of the damping depth constrains soil water release, as shallow drier soil feels the 'squeeze' of atmospheric demand rather than deeper soil that has more water to give up. In this way the diurnally increasing confinement of the gradient to near the rooting plane causes capacitive discharge to collapse, pushing stomata into a feedforward pattern of regulation. This amplification of stress in the soil region nearest the rooting plane then plays an important role in creating the behavior of a

'hydraulic rope' that as the system pulls harder breaks strands rather than pulls more water (Sperry & Love, 2015).

Interpretation of empirical model parameters fit to a diel stationary state

Plotting the instantaneous diurnal values for stomatal conductance against instantaneous *nVPD* (i.e., *nVPD* level multiplied by the diurnal function) results in an apparent stomatal response to *nVPD* (Fig. **7**). Empirical models of plant responses to *VPD* are then fit to these simulated data. Fig. **7a** shows the fit of a *VPD* sensitivity model of the form $g_s = g_{s,ref}$ (1- m ln[$nVPD$]) to the heat wave model output (Oren *et al.* 1999). Typically, this model fits a new $g_{s,ref}$ at a *VPD* of 1 for each quantile of bulk soil moisture, with the slope parameter m then fit within each soil moisture quantile to the response of g_s as *VPD* increases (Novick *et al.*, 2016a). Here, across all four Heat Wave and Control model runs, the bulk soil moisture at the source-edge of the model domain remained the same ($\varphi \sim 2$, $\theta \sim 0.28$, Supplemental Information Fig. **S6)**, justifying the aggregation of all the observations of g_s across all *nVPD* into a single series and fitting a single $g_{s,ref}$ and m. Although not generally discussed, the slope m and intercept $g_{s,ref}$ are highly sensitive to the specific level of *VPD* chosen as a reference, which for the control in the physical heat wave experiment was a *VPD* of about 3 kPa (Drake *et al.*, 2018). Re-basing *nVPD* to the standard reference of 1 kPa results in a value for the slope m of 0.42, consistent with previous estimates for soil moisture limited systems (Oren *et al.*, 1999; Novick *et al.*, 2016a; Grossiord *et al.*, 2020). As there was considerable a.m./p.m. hystersis in the relation of g_s to *nVPD*, the reference value at *nVPD* 1 was $g_{s,ref} = 0.78$, rather than the expected 'stress-free' value of 1: nevertheless the fitted slope of 0.79 picked-out the midday values of g_s as the diurnal spread in values converges at peak stress.

A second semi-empirical approach to modeling *VPD* sensitivity is to consider a steady-state balance between liquid and vapor phase transport mediated by stomatal conductance (Fig. **7b;** Oren *et al.*, 1999; Grossiord *et al.*, 2020; Mencuccini et al., 2024). The notable behavior of this model is that as *VPD* changes, mass balance forces g_s to fall as 1/*vpd*. For the simulations here, the steady mass-balance between soil and atmospheric fluxes holds on average over a diel stationary-state leading to the form $g_s = g_{s,ref} / nVPD$ (Fig. **7b**; derivation in Supplemental Notes **S1**). Fit to the same time-dependent simulated data as the log-based model, the mass-balance model also tracked the midday/peak stress values of g_s for the same reasons as the log fit. Neither

the log nor mass balance models were preferred based on fit statistics, and both captured the peak-stress relationships between *nVPD* and g_s that are often taken as representative of a system (Martínez-Vilalta *et al.*, 2014; Hochberg *et al.*, 2018; Knipfer *et al.*, 2020).

In general, the log and mass-balance descriptions of *VPD* sensitivity do however predict contrasting behaviors of *E* that here coincide with the physical experiment and model at different time scales (Fig. **8a,b** top panels**)**. For the log-based model, the response of *E* transitions from feedback to feedforward at about 2 *nVPD*, capturing a pattern observed in some leaf-scale gas-exchange experiments (Mott & Parkhurst, 1991), and qualitatively consistent with the diurnal development of feedforward responses in the physical experiment and full model (Figs. **2, 3**; Drake *et al.*, 2018). The behavior of the log-based model as a substitute driver for g_s in place of or in addition to water potential in a time-dependent model could not be evaluated here, as in the log-based approach g_s diverges toward infinity as *nVPD* approaches zero at the nocturnal minimum. Another issue is that the log-based model is a steady-state relationship tasked with reproducing behavior that here derives from transient effects. As a result, the log-based model fails to reproduce the observed conservation of *E* in the full model and experiment (Fig. **8a**). The mass balance approach is also limited as it can *only* reproduce the daily time-averaged behavior, as it predicts a single value of *E* independent of diel variations in *nVPD* (Fig. **8b**).

The log and mass balance models further differ in how they partition stomatal responses between soil moisture and *VPD* (Fig. **8a,b**). In the log-based model, information about soil moisture is split between the reference value $g_{s,\mathrm{ref}}$ and the slope parameter *m* for each quantile of soil moisture (Novick *et al.*, 2016a). From the hydraulic perspective of the full model presented here, as the bulk soil dries static declines in water potential lower the maximum stomatal conductance that would pertain at zero *E*, while non-zero *E* induces a dynamic drop in water potential through the soil (and plant) that helps drives feed-forward stomatal behavior in a time-dependent manner. The log-based model follows this partitioning between static ($g_{s,\mathrm{ref}}$) and time-dependent dynamic (*m*) effects, albeit as steady-state behaviors, yet an apparent pathology of this model structure is that at high *VPD* the model predicts lower g_s at higher soil moisture than at low (dotted lines in Fig. **8a**), cautioning against extrapolation of the model fits even within a system. In the mass balance model, falling J_m as the soil system dries out generates a sequence of curves (Fig. **8b)** that do not cross, but decay toward a slowly converging response to *VPD*. This greater realism

comes at the cost of determining J_m, which requires more and potentially harder to obtain information than bulk soil water status.

Finally, treating the state of the soil and *VPD* as independent variables, as both empirical approaches do, represents a zero-coupling limit of land-atmosphere interactions unlikely to pertain at the time and spatial scales of interest (McColl *et al.*, 2019; McColl & Rigden, 2020). By contrast, for a fully coupled land-atmosphere system in steady-state ETRHEQ/SFE picks out the single surface conductance consistent with the observed RH of the atmospheric boundary layer (Fig. **8c** ; see Supplemental Information Notes **S1** for calculations). At high RH (low VPD) states of SFE, large reductions in initially high values of g_s are associated with small reductions in RH (increases in *VPD*). Yet in this humid limit large changes in g_s are associated with very small changes in E (Fig. **8C**, inset). This behavior approaches that of the thick boundary layer limit of Jarvis & McNaughton (1986) and equilibrium evaporation (Raupach, 2001). For flux tower observations, what appears to be a highly sensitive response of g_s to *VPD* may look more like a case of weak stomatal control when E is plotted against g_s, with very different implications for plant stress.

Limitations and numerical artifacts

The steep non-linearity of the stomatal conductance function in the φ domain (Fig. **1e**) did appear to introduce numerical artifacts in the model solution, most evident as jagged deviations from smooth curves (*e.g.*, Day 1 and 4 minimum g_s in Fig. **3c**). That such features are numerical artifacts could be confirmed by their vanishing for model runs with small variations in the initial conditions, as such variations would not be expected to make any difference in the behavior of the quasi-stationary state from day 3 to 7. Numerical artifacts serious enough to prevent convergence on a solution did constrain the range of $g_s\Psi 50$s relative to different ratios of total daily potential transpiration (0.5 E_p) and max soil flux J_m that could be explored, excluding very high and low values.

Discussion

Limitation of transpiration by an emergent maximum flux may be an intrinsic property of the land surface

The emergence of a steady-state asymptotic (maximum) flux is a general feature of passively driven flow through any media for which increasing driving force feeds back negatively on the conductivity, like plant xylem (Sperry & Love, 2015) or soil (Cowan, 1965; Carminati & Javaux, 2020). Yet, predicting the emergence of steady-state and transient maximum soil fluxes hinges on the availability and scale of plant rooting depth, water table depth, and soil texture data.

Global coverage of the effects of soil texture on critical soil moisture already exists (Wankmüller *et al.*, 2024). Estimating plant rooting depth appears more challenging. Over longer time scales, perennial plant rooting depth, soil water availability and depth to the water table are not independent, and highly responsive to local soil conditions; as a result, plant species is a poor predictor of rooting depth (Fan *et al.*, 2017). Fan *et al.* (2017) describe how root growth follows infiltration depth, or the soil depth reached by the wetting front of meteoric water; if this depth is shallower than the capillary fringe of ground water, a 'dry gap' is created between the rooting zone and deep soil moisture. Some trees obligately produce dimorphic roots, building both a shallow root system to access nutrients and seasonally available precipitation, as well as deep roots that cross the dry gap to reach groundwater and so avoid seasonal droughts (Skelton *et al.*, 2021). Yet most taxa remain dependent on meteoric water in the upper soil layers to support high transpiration rates. For 501 taxa, Fan *et al.* (2017) found maximum rooting depth clusters between ~25 cm and 2 m, with the highest density at 1m, paired with water table depths clustered between 1 and 10 m. Meter-scale dry gaps during drought may then occur for many, if not most, woody plants.

Hydrology can interact with climate to create spatial variation in the distribution of dry gaps as well. Miguez-Macho & Fan (2021) report that 70% global transpiration derives from the rain-fed upper soil layers, with moisture in deeper unsaturated soil and rocks accounting for 18%, locally recharged groundwater a mere 1%, and remotely (i.e., lateral flow) recharged groundwater 10%. The 11% due to groundwater seems likely to be due to dimorphic roots in the capillary fringe of the water table, for which the soil flux would be non-limiting. This leaves the 18% taken up from a deep unsaturated zone as the fraction most likely to be governed by a maximum soil flux, though this fraction may be higher in Mediterranean, semi-arid, and seasonally dry tropics (Miguez-Macho & Fan, 2021).

Instances of soil flux limitation of E may also arise in ecologies far from steady state, such as drought, or, in the case of species with dimorphic rooting strategies, during juvenile establishment phases in which the deep roots have not yet reached the capillary fringe. The Drake *et al.* (2018) experiment may fall into the latter category, as the experimental trees were young 6 m tall Eucalyptus that had been growing in soil for one year after being grown in pots to a size of 2 m. While mature Eucalyptus can grow dimorphic roots to depths below 10 m, the neutron-probe measurements showed that under these young trees the largest changes in soil water content occurred at a depth of only 50 cm, presumably due to root uptake.

Under drought, plant survival depends on the balance of the minimum transpiration rate, as influenced by the degree of stomatal closure achieved and cuticular permeability, and the residual flux from the soil, which, in the presence of a water table at some depth, must ultimately converge with the maximum soil flux. The concept of a maximum soil flux from deep soil moisture may then have application for the analysis of spatial and temporal patterns of plant mortality under drought.

The surprising sufficiency of stomatal conductance as a function of leaf water potential

The analyses presented here demonstrate that a model of stomatal aperture as a function of a single integrative variable – water potential – is sufficient to capture both anisohydric to isohydric transitions (Knipfer *et al*., 2020; Javaux & Carminati 2021) and feedforward responses to *VPD*. This is surprising as it was the failure of leaf water potential ψ_L and g_s to follow a 1:1 relationship in response to VPD and soil drying over physiological time scales that motivated work on the role of chemical signaling in stomatal behavior (Turner *et al.*, 1984, 1985; Gollan *et al.*, 1985; Tardieu & Davies, 1992; McAdam & Brodribb, 2016) and contributed motivation to the development of optimization models as an explanation of stomatal behavior (WUE).

One possible reason for the failure of g_s to track ψ_L over physiological time scales may be that, as in the soil, measurements of bulk leaf water potential may not capture the water status relevant to stomata. Leaf water transport models (Rockwell *et al.*, 2014; Buckley *et al.*, 2017) and measurements with fluorescing nanogel reporters of water potential point to the existence of large (up to MPa scale) gradients in water potential from leaf xylem to the transpiring surface (Jain *et al.*, 2024b,a). Such effects may explain why Anderegg et al. (2017) found that a Ball-Berry based model of stomatal conductance that included both leaf water potential and a *VPD*

sensitivity term was preferred over the models containing one or the other. The suggestion is that the bulk measure of leaf water potential may generally be dominated by leaf tissue that sits close to leaf xylem potential, while the *VPD* sensitivity term captures gradients within the leaf proportional to $gs*VPD/K_m$, such that there was no 'double-counting' as would be expected if bulk leaf water potential corresponded to stomatal water potential (Liu *et al.*, 2020b). In this view, it seems relevant that in an influential series of papers demonstrating the failure of g_s to track ψ_L (Turner *et al.*, 1984, 1985; Gollan *et al.*, 1985), leaf water potential was measured by in-situ psychrometers, a technique subsequently shown to track covered leaf water potentials (as measured by the pressure chamber) that represent stem xylem potential at the point of leaf insertion (Matzner & Comstock, 2001).

A further factor that could decouple bulk leaf water potential from the humidity at the sites of evaporation is the development of unsaturation in the leaf air spaces (Márquez *et al.*, 2024; Cernusak *et al.*, 2024; Diao *et al.*, 2024). Yet, as noted by Grossiord et al. (2020), this effect should be fully reflected in parameter observations, that then pass through the effect of unsaturation to deliver ultimately correct predictions of stomatal responses. A similar robustness could characterize the relationship between stomatal conductance and leaf water potential when observations are aggregated and averaged over longer periods than the physiological time scales showing marked hysteresis (i.e., Levin et al., 2019 versus Gollan et al., 1985; Mott & Parkhurst, 1991).

Biological vs physical controls on surface conductance and empirical model parameters

Mott and Parkhurst (1991) showed that stomata respond to *E* rather than directly to *VPD* or RH at the leaf surface. Some sensitive species can show feedforward responses to *VPD* imposed in single leaf cuvettes on well-watered plants, with the degree of sensitivity evidently linked to leaf turgor and ABA (McAdam & Brodribb 2016), but most show limited increases in *E* consistent with feedback type regulation (Mott & Parkhurst 1991; Franks *et al.*, 1997; Franks & Farquhar 1999). Currently there is no complete description of the mechanisms within a leaf that are involved in feedforward and feedback type stomatal responses to *VPD* (Grossiord *et al*, 2020). The evident ability of the physical 'null' model in this study to generate these behaviors does not mean that biology does not matter for VPD responses. Rather, a successful null model is useful for exposing what biological parameters are likely to matter most. With respect to mechanistic

drivers of the empirical parameters in the log-based model, m and g_{ref} are responsive to different physical forcings originating from different moisture states within the same soil (rhizosphere vs bulk). Yet these parameters may be further uncoupled across species, soil textures and systems by biological factors like variations in root density, hairiness and root exudation that impact the scale and degree of soil-root contact (Carminati *et al.*, 2009, 2016; Wankmüller *et al.*, 2024; Akale *et al.*, 2025). It may then be reasonable to consider m as a biologically influenced parameter (with some species specificity) independent of bulk soil moisture and g_{ref}. While root-soil contact was not modeled here, such effects might be detected as an alternative model that better fits experimental data than a continuum model assuming perfect soil-root contact (Herkelrath *et al.*, 1977).

From the perspective of optimization models of stomatal conductance, feedforward behavior and midday closure have been interpreted as conserving a target proportionality between carbon gain and water loss (Novick *et al.*, 2016b; Anderegg *et al.*, 2017; Dewar *et al.*, 2018; Wang *et al.*, 2020; Gardner *et al.*, 2023). In the 'null' model presented here, if one allows the assumption that the daily growth of a non-saturating (at the canopy level) absorbed radiation follows the diurnal curve, feedforward behavior is decidedly sub-optimal as it derives from the decay of excessive rates of water loss in the a.m. The suggestion is not that stomatal behavior in no-way optimizes instantaneous water-use efficiency, rather that optimization may also occur over longer time scales through, for example, adjustments of root-to-shoot ratio, root depth, or soil-root contact that effectively decrease β and so better align the daily courses of stomatal conductance and irradiance by eliminating premature peaking.

Stomatal responses to VPD and the control of transpiration

Outside well-stirred leaf cuvettes and whole plant chambers as in the experiment modeled here, the mechanistic connections between E, VPD, and g_s can become ‘decoupled’ by boundary layer resistances that become competitive with stomatal resistance and cause leaf temperatures to diverge from that of the ambient air (Jarvis & McNaughton, 1986). In the ‘de-coupled limit’ of a thick boundary layer at the canopy scale in Jarvis & McNaughton (1986), large changes in stomatal aperture achieve only small changes in transpiration.

SFE also predicts that at high RH in the ABL large reductions in surface conductance are associated with only small reductions in E. Notably, as the model evolves to a steady state,

changes in RH in the ABL feedback on transpiration as a change in driving force, but there is no feedback of RH on the value of the surface conductance built into the model. That SFE can explain ETRHEQ and patterns of g_s versus *VPD* from flux tower data (McColl & Rigden, 2020) suggests that over these time and spatial scales the relationship between g_s and *VPD* may not be driven by physiological feed-backs of *VPD* on g_s. In the moist land surface and atmosphere limit, the important intuition that emerges is not that g_s is highly sensitive to a stress imposed by atmospheric aridity, but that g_s exerts weak control over the evaporative flux.

In the dry limit, the apparent sensitivity of g_s to *VPD* is less, but the point about the sufficiency of a theory lacking a feedback of *VPD* on g_s still pertains. While for mesic systems flux tower data for *VPD* responses at the daily time scale show a single curve across all soil moisture quantiles as expected by ETRHEQ/SFE (Novick *et al*., 2016a), arid systems tend to show a family of curves comparable to the response of empirical models described here (Fig. **8**). This difference may arise due to drier systems requiring longer than daily time scales to reach SFE (McColl & Rigden, 2020). Once at SFE, the ETRHEQ/SFE hypothesis says there is a unique empirical relationship between g_s and atmospheric RH that emerges from the balance of surface fluxes that may or may not contain information about plant biological responses beyond their basic behavior as physical materials that, like the soil, decline in conductance as their water content drops (Vargas Zeppetello *et al.*, 2023). Under the drier conditions where stomata clearly play an important role in the coupling observed between the atmosphere and land surface, their behavior may be as physically constrained as the formation of a soil crust.

Even if so constrained, stomata play an important role in determining the balance of moisture and heat fluxes, as they represent a resistance seen by latent but not sensible heat, breaking the symmetry between these two energy fluxes that are otherwise coupled by leaf temperature (Cowan & Troughton, 1971). If one adds to this picture the tendency for maximum fluxes to arise from both soil and plant xylem, it becomes clear that the emergence of water-limited maximum surface fluxes could contribute a dynamic constraint on g_s that is insensitive to the precise level of atmospheric aridity, and therefore strongly influences the final quasi-equilibrium state. From this perspective, the critical biological plant factors contributing to the partitioning of surface latent and sensible heat fluxes are likely those that mediate root and soil contact

(Carminati *et al.*, 2016) and so influence the maximum flux available to the evaporative surfaces of the canopy, rather than stomatal behavior considered as an autonomous process.

Conclusion

Under concurrent heat wave and drought stress, the influence of *VPD* on stomatal aperture is strongly mediated by the state of the soil. A boundary condition for a maximum flux from a water table to the zone of uptake is introduced into a transient model of soil water transport to capture situations where plant water potentials under drought are observed to return to similar pre-dawn water potentials over successive days. With the addition of stomatal conductance as a function of leaf water potential, the resulting minimal time-dependent hydraulic model captures intra-day feed forward stomatal behavior, an isohydric responses to *VPD*, and conservation of total daily transpiration across days and *VPD* levels as observed in a whole-tree chamber experiment. The emergence of isohydry is driven by a single dimensionless parameter β, the integrated daily balance of potential transpiration to maximum soil supply. Emergence of feedforward regulation E is time-dependent and driven by both β and the soil diffusivity, which is soil texture dependent. While steady-state empirical model parameters can be mapped to hydraulic mechanisms, these reduced models struggle to capture relevant responses of E. These results motivate further investigation into the physical and biological factors controlling the surface conductance of plant canopies coupled to the atmospheric boundary layer.

Acknowledgements

Abraham Stroock, Guido Salvucci, Kaighin McColl, Daniel Short Gianotti and N.M. Holbrook provided valuable feedback and discussion. This work was supported by NSF-MRSEC DMR-2011754.

Competing interests

None declared

Data availability

No new data were generated in this study, and all simulated data are available by evaluating the code given in Supplemental Information Notes **S4**.

Figure legends

Figure **1**. Minimal hydraulic model of the soil-plant-atmosphere continuum. **a** The last ten centimeters of the distance *L* from the water table to rooting depth forms the modeled soil domain, bounded at the lower surface by a maximum flux from the water table J_m, and at the upper surface by a variable root uptake flux equivalent to transpiration *E*, as driven by the product of a diurnal demand function *f(t)* (in **b**) and *nVPD*. **c** Dimensionless stomatal conductance g_s as a function of leaf water potential Ψ [MPa], with the $g_s\Psi 50$ for a 50% decline in stomatal conductance set at -1.33 MPa (dotted lines). In the modeled domain **d**, water content θ depends on soil hydraulic conductivity *K(h)* [cm day^{-1}] and the gradient in matric potential *h* [cm]. **e** Transformation of the water content, matric and water potentials to the potential flux domain [φ, cm^2 day^{-1}] linearizes the governing equation, but at the cost of an extremely steep function for g_s.

Figure **2**. Emergence of feedforward and counter-factual anisohydric behavior in the model for the heat wave experiment in Drake *et al.* (2018) for normalized vapor pressure deficit (*nVPD*) levels of 1 (Control, blue lines) and 2 (Heat Wave, red lines). The first three days (shaded) represent a 'dry-down' from a SMC θ = 0.25 used to initialize the model to a four-day quasi-steady diurnal cycle comparable to the physical experiment. (**a**) Diurnal cycles of *E* for the Heat Wave peak earlier and show feedforward declines relative to the control that conserves total daily *E* (inset bar chart). (**b**) Diurnal cycles of root (dashed) and leaf (solid) water potential Ψ show an anisohydric response across *nVPD* levels as leaf Ψ more than doubles in magnitude. (**c**) Diurnal variations in g_s show minor g_s limitation at *nVPD* 1 while at *nVPD* 2 g_s is forced to below 50% at midday: inset bar chart of integrated total g_s over four days shows that *A* and *E* become decoupled at high *nVPD*.

Figure **3**. Emergence of feedforward and isohydric behavior as observed in the heat wave experiment in Drake *et al*. (2018) for normalized vapor pressure deficit (*nVPD)* levels of 1.25 (Control, blue lines) and 2.5 (Heat Wave, red lines). The first three days (shaded) represent a 'dry-down' from a SMC of θ = 0.25 used to initialize the model to a four-day stationary diurnal cycle comparable to the physical experiment. (**a**) Diurnal cycles of *E* for the Heat Wave peak earlier and show feedforward declines relative to the control that conserve total daily *E* (inset bar chart). (**b**) Diurnal variations in root (dashed) and leaf (solid) water potential create a near 'isohydric response' of Ψ_{leaf} to *nVPD*. (**c**) Diurnal variations in g_s show stomatal limitation at

midday at both *nVPD* levels: inset bar chart of total integrated g_s shows *A* and *E* are more decoupled at higher *nVPD*.

Figure **4**. Effect of doubling $g_s\Psi 50$ ('osmotic adjustment') from -1.33 MPa (**a**,**b**,**c**) to -2.66 MPa (**d**,**e**,**f**) with *nVPD* 1 (blue) and *nVPD* 2 (red). **a,d** Diel course of transpiration in the stationary state: maintaining higher g_s to lower Ψ stretches the a.m. peak, but *E* for both setpoints converges rapidly once stomata start to constrain the water flux. **b**,**e** Gradients of water potential through the soil domain at the nocturnal maximum and diurnal minimum of *nVPD*: the space between the two lines (light blue) for each level of *nVPD* shows the region of the domain subject to daily fluctuations in water content, which remain confined to near the rooting plane (z=10 cm). **c**,**f** Diel course of soil (dashed) and leaf (solid) water potential; at *nVPD* 2 shifting stomatal closure to a value twice as negative allows leaf water potential to fall to values almost twice as dry but fails to pull a larger midday or total daily water flux from the soil (**a**,**d**).

Figure **5.** Emergence of feedforward behavior and isohydry from different aspects of the soil plant system. **a** Parametric sweep across β levels 1 (blue solid), 1.5 (blue dashed), 2 (red dashed) and 5 (red solid) showing the emergence of feedforward behavior at D_o=25.7. **b** Diel course of leaf (solid) and root (dashed) water potentials showing the transition from anisohydric to isohydric for the same simulations as in **a**. **c** Decay of feedforward behavior at β=2.5 as D_o falls from 25.7 (red) to 15 (blue), 5 (black dashed) and 1 (black solid). **d** Diel course of leaf (solid) and root (dashed) water potentials for the simulations in **c** showing no change in the pattern of midday leaf water potentials but greater relaxation at pre-dawn as D_o falls. **e** Parametric sweep across β levels 1 (blue solid), 1.5 (blue dashed), 2 (red dashed) and 2.5 (red solid) showing peak broadening replaces the emergence of feedforward behavior from increasing supply and demand imbalance at D_o=1. **f** The emergence of isohydry at D_o=1 follows the same pattern as at D_o=25.7.

Figure **6**. Diel course of potential transpiration (solid) and actual transpiration *E* (dashed) in the stationary state at β=1 (blue) and β =2 (red), for a soil diffusivity set to 1 $cm^2\ s^{-1}$ (**a**) and 25.7 $cm^2\ s^{-1}$ (**b**); light blue shading indicates periods of net recharge (below the steady inward soil flux J_m) and discharge (above J_m) of the 10 cm deep model domain with respect to the β=2 case, with the heights (solid and dashed arrows respectively) proportional to the magnitude of the recharge/discharge flux at that instant. Note the total areas under all the dashed lines are approximately equal. **c**,**d**,**e**,**f**: Gradients in water potential through the soil domain to the root

plane at z=10 at the daily minimum and maximums of *E*; the intervening space (light blue) shows the region and potential range for transient release of water over this period (note the difference in potential scales), relative to the damping depth δ, which represents how far into the soil domain diel variations are expected to reach. Panels **c,d** correspond to **a,** and **e,f** to **b.** Note that differences in areas between the gradients (light blue) across **c**,**d**,**e**,**f** cannot be simply interpreted as differences in the volumes of water released due to differences in scale.

Figure **7**. Fits of simulated diurnal values (hysteretic loops) of stomatal conductance for two contrasting models of stomatal sensitivity to *VPD.* Data are for all four modeled *nVPD* levels (cyan 1, green 1.25, red 2, blue 2.5); black solid lines show the fit and dashed lines the 99% CI. **a** Log-based model: $g_s = g_{s,ref}\,(1 - m \ln[nVPD])$, $g_{s,ref} = 0.78$, $m = 0.79$, adj$R^2 = 0.96$. **b** Mass-balance based model: $g_s = g_{s,ref}/nVPD$, $g_{s,ref} = 0.78$, adj$R^2 = 0.96$.

Figure **8**. A comparison of the normalized conductance extinction curves ($g_s/g_{s,ref}$) and transpiration responses (E/E_{ref}) for three simplified models of stomatal responses to soil drying and atmospheric aridity, with 1 kPa as the reference state for *nVPD*. **a** Based on the behavior of the dry sites in figure 2 of Novick *et al.* (2016), as the soil dries in the model $g_s/g_{s,ref} = a\,(1 - m \ln[nVPD])$ the intercept *a* falls from 1 at *nVPD* =1 to 0.2 while the slope *m* falls from 0.6 to 0.2. Note that the curves representing *nVPD* responses at higher soil moisture are predicted to cross (at the transition from solid to dashed) the curves for lower soil moisture. **b** For the mass balance model $g_s/g_{s,ref} = (J_m/J_{m,ref})\,(1/nVPD)$, $J_m/J_{m,ref}$ falls from 1 to 0.2 to simulate a falling maximum flux as the soil dries. **c** Under the condition of Surface Flux Equilibrium (SFE), the atmospheric boundary layer approaches a constant RH (and potential *nVPD*) at all heights; responses are shown for air temperatures at two meters above the canopy of 280, 300 and 320 K.

References

Akale A, Abdalla M, Koehler T, Sauer AM, Diamantopoulos E, Ahmed MA. **2025**. Root mucilage enhances plant water use under combined soil and atmospheric drought. *Annals of Botany*.

Anderegg WRL, Wolf A, Arango-Velez A, Choat B, Chmura DJ, Jansen S, Kolb T, Li S, Meinzer F, Pita P, *et al.* 2017. Plant water potential improves prediction of empirical stomatal models. *PLoS ONE* **12**.

Attia Z, Domec JC, Oren R, Way DA, Moshelion M. **2015**. Growth and physiological responses of isohydric and anisohydric poplars to drought. *Journal of Experimental Botany* **66**: 4373–4381.

Berg A, Sheffield J. **2018**. Climate Change and Drought: the Soil Moisture Perspective. *Current Climate Change Reports* **4**: 180–191.

Binks O, Cernusak LA, Liddell M, Bradford M, Coughlin I, Carle H, Bryant C, Dunn E, Oliveira R, Mencuccini M, *et al.* 2022. Forest system hydraulic conductance: partitioning tree and soil components. *New Phytologist* **233**: 1667–1681.

Brodribb TJ, & Holbrook NM. 2003. Stomatal closure during leaf dehydration, correlation with other leaf physiological traits. *Plant Physiology* **132**: 2166–2173. https://doi.org/10.1104/pp.103.023879

Brodribb TJ, McAdam SAM. **2011**. Passive origins of stomatal control in vascular plants. *Science* **331**: 582–585.

Buckley TN. **2005**. The control of stomata by water balance. *New Phytologist* **168**: 275–292.

Buckley TN. **2019**. How do stomata respond to water status? *New Phytologist* **224**: 21–36.

Buckley TN, John GP, Scoffoni C, Sack L. **2017**. The sites of evaporation within leaves. *Plant Physiology* **173**: 1763–1782.

Carminati A, Javaux M. **2020**. Soil Rather Than Xylem Vulnerability Controls Stomatal Response to Drought. *Trends in Plant Science* **25**: 868–880.

Carminati A, Vetterlein D, Weller U, Vogel H-J, Oswald SE. **2009**. When Roots Lose Contact. *Vadose Zone Journal* **8**: 805–809.

Carminati A, Zarebanadkouki M, Kroener E, Ahmed MA, Holz M. **2016**. Biophysical rhizosphere processes affecting root water uptake. *Annals of Botany* **118**: 561–571.

Cernusak LA, Wong SC, Stuart-Williams H, Márquez DA, Pontarin N, Farquhar GD. **2024**. Unsaturation in the air spaces of leaves and its implications. *Plant Cell and Environment*.

Cowan IR. **1965**. Transport of Water in the Soil-Plant-Atmosphere System. *Journal of Applied Ecology* **2**: 221–239.

Cowan IR, Troughton GH. **1971**. The Relative Role of Stomata in Transpiration and Assimilation. *Planta* **97**: 325–336.

Dawson TE, Hahm WJ, Crutchfield-Peters K. **2020**. Digging deeper: what the critical zone perspective adds to the study of plant ecophysiology. *New Phytologist* **226**: 666–671.

Dewar R, Mauranen A, Mäkelä A, Hölttä T, Medlyn B, Vesala T. **2018**. New insights into the covariation of stomatal, mesophyll and hydraulic conductances from optimization models incorporating nonstomatal limitations to photosynthesis. *New Phytologist* **217**: 571–585.

Diao H, Cernusak LA, Saurer M, Gessler A, Siegwolf RTW, Lehmann MM. **2024**. Dry inside: progressive unsaturation within leaves with increasing vapour pressure deficit affects estimation of key leaf gas exchange parameters. *New Phytologist* **244**: 1275–1287.

Drake JE, Tjoelker MG, Vårhammar A, Medlyn BE, Reich PB, Leigh A, Pfautsch S, Blackman CJ, López R, Aspinwall MJ, *et al.* 2018. Trees tolerate an extreme heatwave via sustained transpirational cooling and increased leaf thermal tolerance. *Global Change Biology* **24**: 2390–2402.

Fan Y, Miguez-Macho G, Jobbágy EG, Jackson RB, Otero-Casal C. **2017**. Hydrologic regulation of plant rooting depth. *Proceedings of the National Academy of Sciences of the United States of America* **114**: 10572–10577.

Feng X, Ackerly DD, Dawson TE, Manzoni S, McLaughlin B, Skelton RP, Vico G, Weitz AP, Thompson SE. **2019**. Beyond isohydricity: The role of environmental variability in determining plant drought responses. *Plant Cell and Environment* **42**: 1104–1111.

Franks PJ, Cowan IR, Farquhar GD. **1997**. The apparent feedforward response of stomata to air vapour pressure deficit: Information revealed by different experimental procedures with two rainforest trees. *Plant, Cell and Environment* **20**: 142–145.

Franks PJ, & Farquhar GD. 1999. A relationship between humidity response, growth form and photosynthetic operating point in C3 plants. *Plant, Cell and Environment* **22**: 1337–1349.

Franks PJ, Farquhar GD. **2007**. The mechanical diversity of stomata and its significance in gas-exchange control. *Plant Physiology* **143**: 78–87.

Gardner W. **1958**. Some steady-state solutions of the unsaturated flow equation with application to evaporation from a water table. *Soil Science* **85**: 228–232.

Gardner W, Fireman M. **1958**. Laboratory studies of evaporation from soil columns in the presence of a water table. *Soil Science* **85**: 244–249.

Gardner A, Jiang M, Ellsworth DS, MacKenzie AR, Pritchard J, Bader MKF, Barton CVM, Bernacchi C, Calfapietra C, Crous KY, *et al.* 2023. Optimal stomatal theory predicts CO2 responses of stomatal conductance in both gymnosperm and angiosperm trees. *New Phytologist* **237**: 1229–1241.

Gollan T, Turner NC, Schulze E-D. **1985**. The responses of stomata and leaf gas exchange to vapour pressure deficits and soil water content III. In the sclerophyllous woody species Nerium oleander. *Oecologia* **65**: 356–362.

Grossiord C, Buckley TN, Cernusak LA, Novick KA, Poulter B, Siegwolf RTW, Sperry JS, McDowell NG. **2020**. Plant responses to rising vapor pressure deficit. *New Phytologist* **226**: 1550–1566.

Herkelrath WN, Miller EE, Gardner WR. **1977**. Water uptake by plants II: The root contact model. *Soil Science* **41**: 1039–1043.

Hochberg U, Rockwell FE, Holbrook NM, Cochard H. **2018**. Iso/Anisohydry: A Plant–Environment Interaction Rather Than a Simple Hydraulic Trait. *Trends in Plant Science* **23**: 112–120.

Van Den Honert TH. **1948**. Water transport in plants as a catenary process. *Discussions of the Faraday Society* **3**: 146–153.

Hunt, Jr. ER, Qu JJ, Hao X, Wang L. **2009**. Remote sensing of canopy water content: scaling from leaf data to MODIS. In: Remote Sensing and Modeling of Ecosystems for Sustainability VI. SPIE, 745409.

Jain P, Huber AE, Rockwell FE, Sen S, Holbrook NM, Stroock AD. **2024a**. Localized measurements of water potential reveal large loss of conductance in living tissues of maize leaves. *Plant Physiology* **194**: 2288–2300.

Jain P, Huber AE, Rockwell FE, Sen S, Holbrook NM, Stroock AD. **2024b**. New approaches to dissect leaf hydraulics reveal large gradients in living tissues of tomato leaves. *New Phytologist* **242**: 453–465.

Jarvis P, McNaughton K. **1986**. Stomatal control of transpiration: Scaling up from leaf to region. In: MacFadyen A, Ford E, eds. Advances in Ecological Research. London: Academic Press, 1–45.

Javaux M, Carminati A. **2021**. Soil hydraulics affect the degree of isohydricity. *Plant Physiology* **186**: 1378–1381.

Jezek M, Blatt MR. **2017**. The membrane transport system of the guard cell and its integration for stomatal dynamics. *Plant Physiology* **174**: 487–519.

Jezek M, Hills A, Blatt MR, Lew VL. **2019**. A constraint–relaxation–recovery mechanism for stomatal dynamics. *Plant Cell and Environment* **42**: 2399–2410.

Jury WA, Gardner WR, Gardner WH. **1991**. *Soil Physics*. New York: Wiley.

Knipfer T, Bambach N, Isabel Hernandez M, Bartlett MK, Sinclair G, Duong F, Kluepfel DA, McElrone AJ. **2020**. Predicting stomatal closure and turgor loss in woody plants using predawn and midday water potential. *Plant Physiology* **184**: 881–894.

Koehler T, Botezatu Á, Murugesan T, Kaliamoorthy S, Kholová J, Sadok W, Ahmed MA, Carminati A. **2024**. The transpiration rate sensitivity to increasing evaporative demand differs between soil textures, even in wet soil. *Plant Stress* **12**.

Konings AG, Gentine P. **2017**. Global variations in ecosystem-scale isohydricity. *Global Change Biology* **23**: 891–905.

Levin AD, Williams LE, Matthews MA. **2019**. A continuum of stomatal responses to water deficits among 17 wine grape cultivars (Vitis vinifera). *Functional Plant Biology* **47**: 11–25.

Liu L, Gudmundsson L, Hauser M, Qin D, Li S, Seneviratne SI. **2020a**. Soil moisture dominates dryness stress on ecosystem production globally. *Nature Communications* **11**.

Liu Y, Kumar M, Katul GG, Feng X, Konings AG. **2020b**. Plant hydraulics accentuates the effect of atmospheric moisture stress on transpiration. *Nature Climate Change* **10**: 691–695.

Manandhar A, Rimer IM, Soares Pereira T, Pichaco J, Rockwell FE, McAdam SAM. **2024**. Dynamic soil hydraulic resistance regulates stomata. *New Phytologist* **244**: 147–158.

Márquez DA, Wong SC, Stuart-Williams H, Cernusak LA, Farquhar GD. **2024**. Mesophyll airspace unsaturation drives C4 plant success under vapor pressure deficit stress. *Proceedings of the National Academy of Sciences of the United States of America* **121**.

Martínez-Vilalta J, Garcia-Forner N. **2017**. Water potential regulation, stomatal behaviour and hydraulic transport under drought: deconstructing the iso/anisohydric concept. *Plant Cell and Environment* **40**: 962–976.

Martínez-Vilalta J, Poyatos R, Aguadé D, Retana J, Mencuccini M. **2014**. A new look at water transport regulation in plants. *New Phytologist* **204**: 105–115.

Matusick G, Ruthrof KX, Kala J, Brouwers NC, Breshears DD, Hardy GESJ. **2018**. Chronic historical drought legacy exacerbates tree mortality and crown dieback during acute heatwave-compounded drought. *Environmental Research Letters* **13**.

Matzner S, Comstock J. **2001**. The temperature dependence of shoot hydraulic resistance: Implications for stomatal behavior and hydraulic limitation. *Plant, Cell and Environment* **24**: 1299–1307.

McAdam SAM, Brodribb TJ. **2016**. Linking turgor with ABA biosynthesis: Implications for stomatal responses to vapor pressure deficit across land plants. *Plant Physiology* **171**: 2008–2016.

McColl KA, Rigden AJ. **2020**. Emergent Simplicity of Continental Evapotranspiration. *Geophysical Research Letters* **47**.

McColl KA, Salvucci GD, Gentine P. **2019**. Surface Flux Equilibrium Theory Explains an Empirical Estimate of Water-Limited Daily Evapotranspiration. *Journal of Advances in Modeling Earth Systems* **11**: 2036–2049.

McColl KA, Tang LI. **2024**. An Analytic Theory of Near-Surface Relative Humidity over Land. *Journal of Climate* **37**: 1213–1230.

McCully ME, McCully JSB, And Boyer ME. **1997**. The expansion of maize root-cap mucilage during hydration. 3. Changes in water potential and water content. *Physiologia Plantarum* **99**: 169–177.

Mencuccini M, Anderegg WRL, Binks O, Knipfer T, Konings AG, Novick K, Poyatos R, Martínez-Vilalta J. **2024**. A new empirical framework to quantify the hydraulic effects of soil and atmospheric drivers on plant water status. *Global Change Biology* **30**.

Messinger SM, Buckley TN, Mott KA. **2006**. Evidence for involvement of photosynthetic processes in the stomatal response to CO2. *Plant Physiology* **140**: 771–778.

Miguez-Macho G, Fan Y. **2021**. Spatiotemporal origin of soil water taken up by vegetation. *Nature* **598**: 624–628.

Mitchell PJ, O'Grady AP, Hayes KR, Pinkard EA. **2014**. Exposure of trees to drought-induced die-off is defined by a common climatic threshold across different vegetation types. *Ecology and Evolution* **4**: 1088–1101.

Mott KA, Parkhurst DF. **1991**. Stomatal responses to humidity in air and helox. *Plant, Cell & Environment* **14**: 509–515.

Mrad A, Sevanto S, Domec JC, Liu Y, Nakad M, Katul G. **2019**. A dynamic optimality Principle for water use strategies explains isohydric to anisohydric plant responses to drought. *Frontiers in Forests and Global Change* **2**.

Novick KA, Ficklin DL, Grossiord C, Konings AG, Martínez-Vilalta J, Sadok W, Trugman AT, Williams AP, Wright AJ, Abatzoglou JT, *et al.* 2024. The impacts of rising vapour pressure deficit in natural and managed ecosystems. *Plant Cell and Environment* **47**: 3561–3589.

Novick KA, Ficklin DL, Stoy PC, Williams CA, Bohrer G, Oishi AC, Papuga SA, Blanken PD, Noormets A, Sulman BN, *et al.* 2016a. The increasing importance of atmospheric demand for ecosystem water and carbon fluxes. *Nature Climate Change* **6**: 1023–1027.

Novick KA, Konings AG, Gentine P. **2019**. Beyond soil water potential: An expanded view on isohydricity including land–atmosphere interactions and phenology. *Plant Cell and Environment* **42**: 1802–1815.

Novick KA, Miniat CF, Vose JM. **2016b**. Drought limitations to leaf-level gas exchange: Results from a model linking stomatal optimization and cohesion-tension theory. *Plant Cell and Environment* **39**: 583–596.

Oren R, Sperry JS, Katul GG, Pataki DE, Ewers BE, Phillips N, Schäfer KVR. **1999**. Survey and synthesis of intra- and interspecific variation in stomatal sensitivity to vapour pressure deficit. *Plant, Cell and Environment* **22**: 1515–1526.

Philip J. **1957**. The Physical Principles of soil water movement during the irrigation cycle. In: Proceedings of 3rd International Commission on Irrigation and Drainage. 125–154.

Philip JR. **1966**. Plant water relations: some physical aspects. *Annual Review of Plant Biology* **17**: 245–268.

Raupach MR. **2001**. Combination theory and equilibrium evaporation. *Quarterly Journal of the Royal Meteorological Society* **127**: 1149–1181.

Rigden AJ, Salvucci GD. **2015**. Evapotranspiration based on equilibrated relative humidity (ETRHEQ): Evaluation over the continental U.S. *Water Resources Research* **51**: 2951–2973.

Rockwell FE, Holbrook NM, Stroock AD. **2014**. The competition between liquid and vapor transport in transpiring leaves. *Plant Physiology* **164**: 1741–1758.

Roderick ML, Greve P, Farquhar GD. **2015**. On the assessment of aridity with changes in atmospheric CO2. *Water Resources Research* **51**: 5450–5463.

Rodriguez-Dominguez CM, Brodribb TJ. **2020**. Declining root water transport drives stomatal closure in olive under moderate water stress. *New Phytologist* **225**: 126–134.

Salvucci GD, Gentine P. **2013**. Emergent relation between surface vapor conductance and relative humidity profiles yields evaporation rates from weather data. *Proceedings of the National Academy of Sciences of the United States of America* **110**: 6287–6291.

Schroeder JI, Allen GJ, Hugouvieux V, Kwak JM, Waner D. **2001**. Guard Cell Signal Transduction. *Annu. Rev. Plant Physiol. Plant Mol. Biol* **52**: 627–58.

Scoffoni C, Albuquerque C, Brodersen CR, Townes S V., John GP, Bartlett MK, Buckley TN, McElrone AJ, Sack L. **2017**. Outside-xylem vulnerability, not Xylem embolism, controls leaf hydraulic decline during dehydration. *Plant Physiology* **173**: 1197–1210.

Shatil-Cohen A, Attia Z, Moshelion M. **2011**. Bundle-sheath cell regulation of xylem-mesophyll water transport via aquaporins under drought stress: A target of xylem-borne ABA? *Plant Journal* **67**: 72–80.

Shiklomanov I. **1993**. World Freshwater Resources. In: Gleick PH, ed. Water in Crisis: A Guide to the World's Freshwater Resources. New York: Oxford University Press.

Simonneau T, Tardieu F. **1998**. Variability among species of stomatal control under fluctuating soil water status and evaporative demand: modelling isohydric and anisohydric behaviours. *Journal of Experimental Botany* **49**: 419–432.

Skelton RP, Anderegg LDL, Diaz J, Kling MM, Papper P, Lamarque LJ, Delzon S, Dawson TE, Ackerly DD. **2021**. Evolutionary relationships between drought-related traits and climate shape large hydraulic safety margins in western North American oaks. *Proceedings of the National Academy of Sciences of the United States of America* **118**.

Sloan BP, Thompson SE, Feng X. **2021**. Plant hydraulic transport controls transpiration sensitivity to soil water stress. *Hydrology and Earth System Sciences* **25**: 4259–4274.

Sperry JS, Adler F, Campbell G, Comstock J. **1998**. Limitation of plant water use by rhizosphere and xylem conductance: results from a model. *Plant, Cell and Environment* **21**: 347–359.

Sperry JS, Love DM. **2015**. What plant hydraulics can tell us about responses to climate-change droughts. *New Phytologist* **207**: 14–27.

Tardieu F, Davies WJ. **1992**. Stomatal response to abscisic acid is a function of current plant water status. *Plant Physiology* **98**: 540–545.

Tardieu F, Simonneau T. **1998**. Variability among species of stomatal control under fluctuating soil water status and evaporative demand: modelling isohydric and anisohydric behaviours. *Journal of Experimental Botany* **49**: 419–432.

Turner NC, Schulze E-D, Gollan T. **1984**. The responses of stomata and leaf gas exchange to vapour pressure deficits and soil water content I. Species comparisons at high soil water contents. *Oecologia* **63**: 338–342.

Turner NC, Schulze E-D, Gollan T. **1985**. The responses of stomata and leaf gas exchange to vapour pressure deficits and soil water content II. In the mesophytic herbaceous species Helianthus annuus. *Oecologia* **65**: 348.

Tuzet A, Perrier A, Leuning R. **2003**. A coupled model of stomatal conductance, photosynthesis and transpiration. *Plant, Cell and Environment* **26**: 1097–1116.

Vargas Zeppetello LR, McColl KA, Bernau JA, Bowen BB, Tang LI, Holbrook NM, Gentine P, Huybers P. **2023**. Apparent surface conductance sensitivity to vapour pressure deficit in the absence of plants. *Nature Water* **1**: 941–951.

Wang Y, Sperry JS, Anderegg WRL, Venturas MD, Trugman AT. **2020**. A theoretical and empirical assessment of stomatal optimization modeling. *New Phytologist* **227**: 311–325.

Wankmüller FJP, Carminati A. **2022**. Stomatal regulation prevents plants from critical water potentials during drought: Result of a model linking soil–plant hydraulics to abscisic acid dynamics. *Ecohydrology* **15**.

Wankmüller FJP, Delval L, Lehmann P, Baur MJ, Cecere A, Wolf S, Or D, Javaux M, Carminati A. **2024**. Global influence of soil texture on ecosystem water limitation. *Nature* **635**: 631–638.

Wu G, Guan K, Li Y, Novick KA, Feng X, McDowell NG, Konings AG, Thompson SE, Kimball JS, De Kauwe MG, *et al.* 2021. Interannual variability of ecosystem iso/anisohydry is regulated by environmental dryness. *New Phytologist* **229**: 2562–2575.

Zhang YJ, Rockwell FE, Graham AC, Alexander T, Holbrook NM. **2016**. Reversible leaf xylem collapse: A potential 'circuit breaker' against cavitation. *Plant Physiology* **172**: 2261–2274.

Supplemental Information

Notes **S1**. Derivations.

Figure **S2**. Maximum soil fluxes for fine sandy loam and clay soils.

Figure **S3.** Maximum soil flux for the light clay soil used in the model.

Notes **S4**. Computer code for model runs and figures.

Figure **S5**. Supply curve for a clay soil as the rooting plane dries.

Figure **S6**. Evolution of the potential flux φ for all modeled levels of *nVPD*.

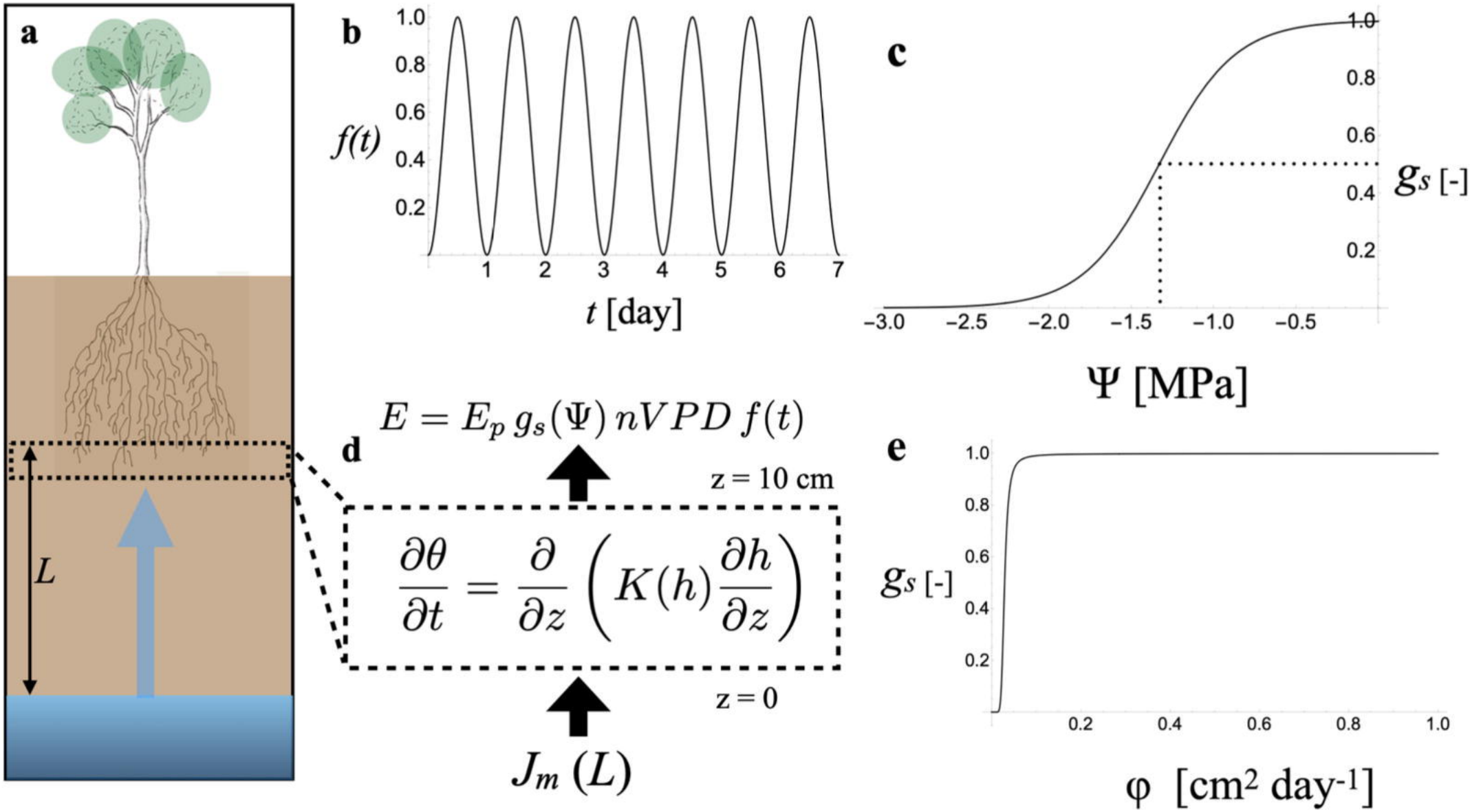

Figure **1**. Minimal hydraulic model of the soil-plant-atmosphere continuum. **a** The last ten centimeters of the distance L from the water table to rooting depth forms the modeled soil domain, bounded at the lower surface by a maximum flux from the water table J_m, and at the upper surface by a variable root uptake flux equivalent to transpiration E, as driven by the product of a diurnal demand function $f(t)$ (in **b**) and $nVPD$. **c** Dimensionless stomatal conductance g_s as a function of leaf water potential Ψ [MPa], with the $g_s\Psi 50$ for a 50% decline in stomatal conductance set at -1.33 MPa (dotted lines). In the modeled domain **d**, water content θ depends on soil hydraulic conductivity $K(h)$ [cm day^{-1}] and the gradient in matric potential h [cm]. **e** Transformation of the water content, matric and water potentials to the potential flux domain [φ, cm^2 day^{-1}] linearizes the governing equation, but at the cost of an extremely steep function for g_s.

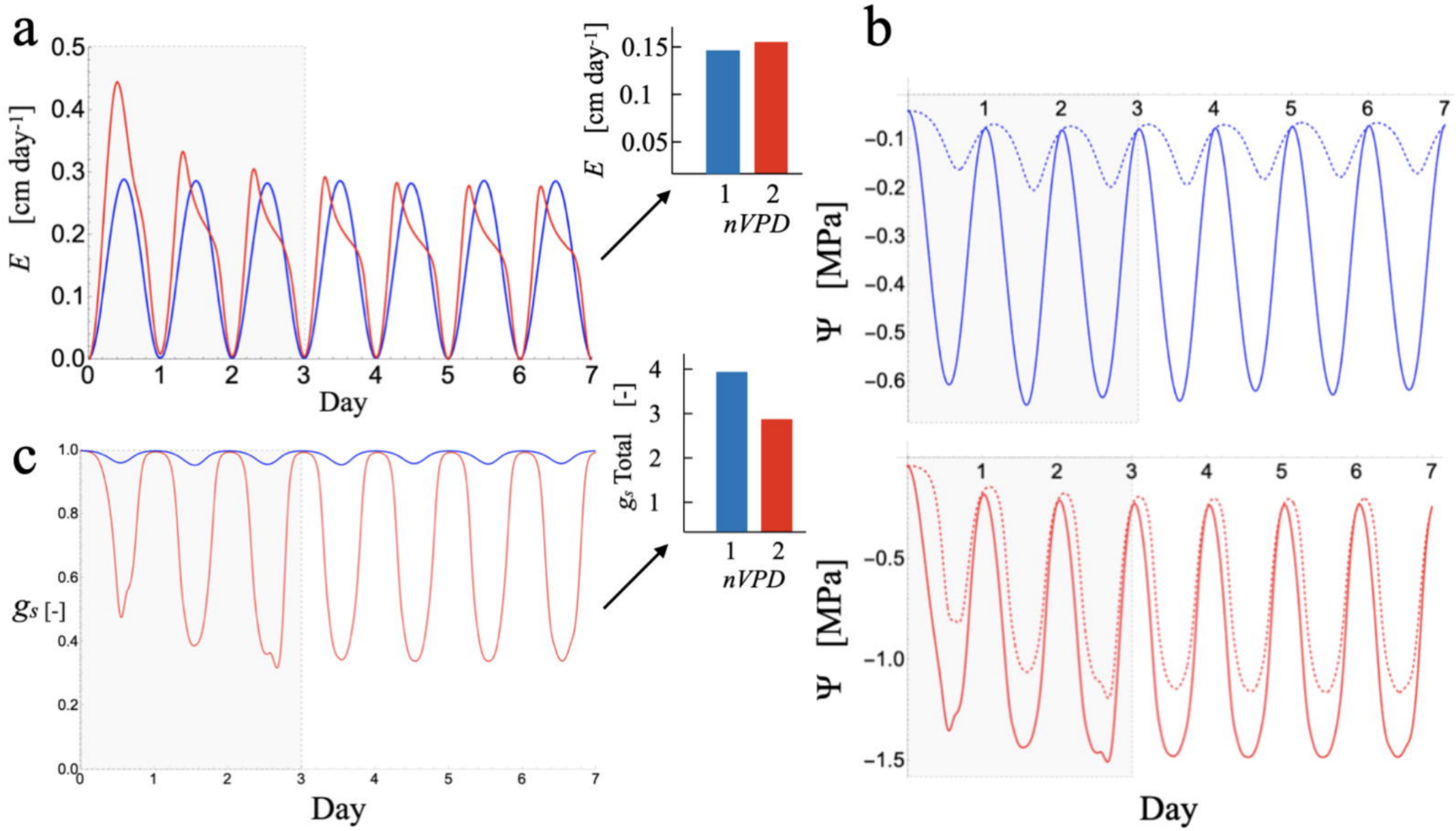

Figure **2**. Emergence of feedforward and counter-factual anisohydric behavior in the model for the heat wave experiment in Drake *et al.* (2018) for normalized vapor pressure deficit (*nVPD*) levels of 1 (Control, blue lines) and 2 (Heat Wave, red lines). The first three days (shaded) represent a 'dry-down' from a SMC $\theta = 0.25$ used to initialize the model to a four-day quasi-steady diurnal cycle comparable to the physical experiment. (**a**) Diurnal cycles of E for the Heat Wave peak earlier and show feed-forward declines relative to the control that conserves total daily E (inset bar chart). (**b**) Diurnal cycles of root (dashed) and leaf (solid) water potential Ψ show an anisohydric response across *nVPD* levels as leaf Ψ more than doubles in magnitude. (**c**) Diurnal variations in g_s show minor g_s limitation at *nVPD* 1 while at *nVPD* 2 g_s is forced to below 50% at midday: inset bar chart of integrated total g_s over four days shows that A and E become decoupled at high *nVPD*.

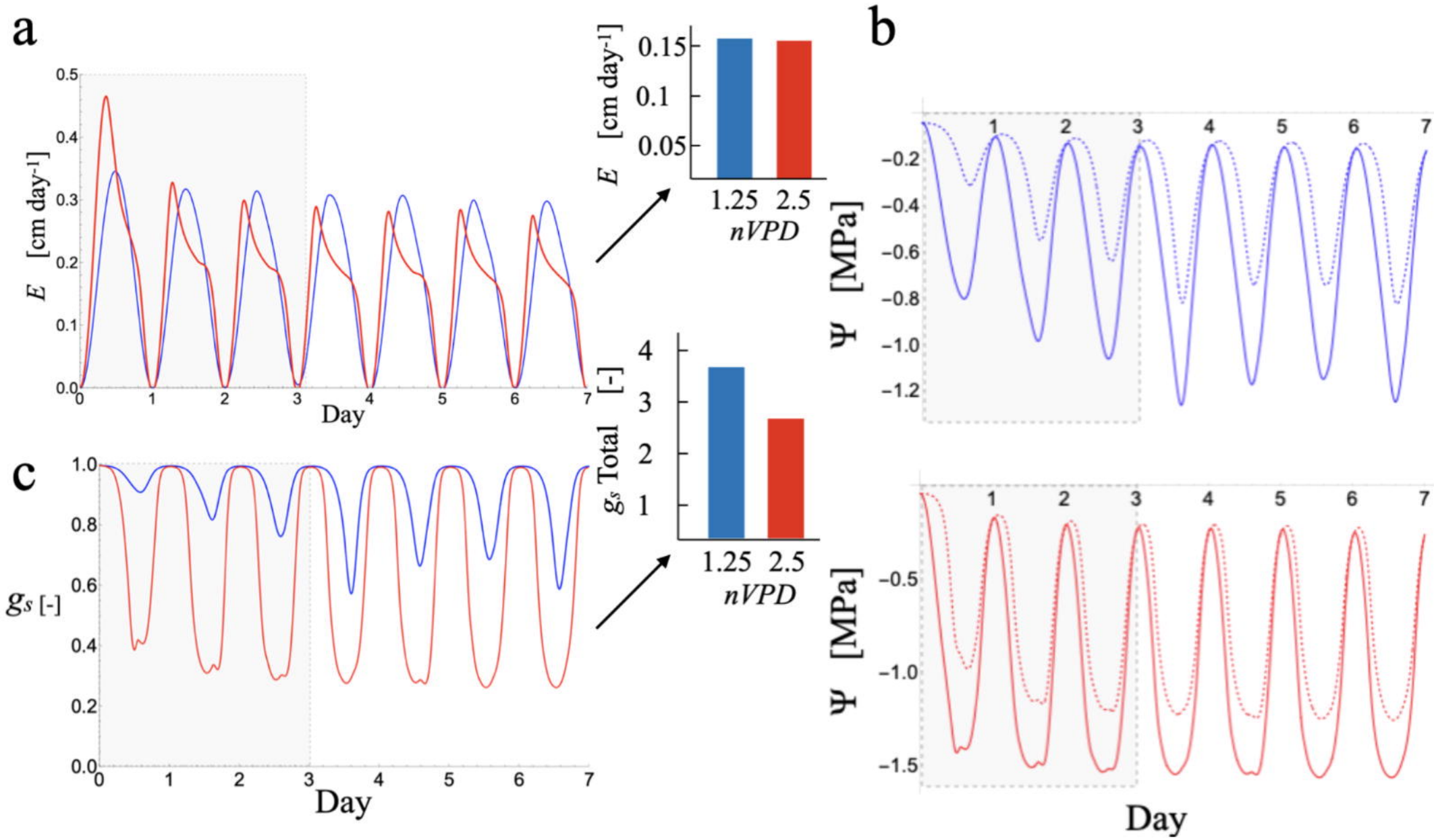

Figure **3**. Emergence of feedforward and isohydric behavior as observed in the heat wave experiment in Drake *et al.* (2018) for normalized vapor pressure deficit (*nVPD)* levels of 1.25 (Control, blue lines) and 2.5 (Heat Wave, red lines). The first three days (shaded) represent a 'dry-down' from a SMC of $\theta = 0.25$ used to initialize the model to a four-day stationary diurnal cycle comparable to the physical experiment. (**a**) Diurnal cycles of E for the Heat Wave peak earlier and show feedforward declines relative to the control that conserve total daily E (inset bar chart). (**b**) Diurnal variations in root (dashed) and leaf (solid) water potential create a near 'isohydric response' of Ψ_{leaf} to *nVPD*. (**c**) Diurnal variations in g_s show stomatal limitation at midday at both *nVPD* levels: inset bar chart of total integrated g_s shows A and E are more decoupled at higher *nVPD*.

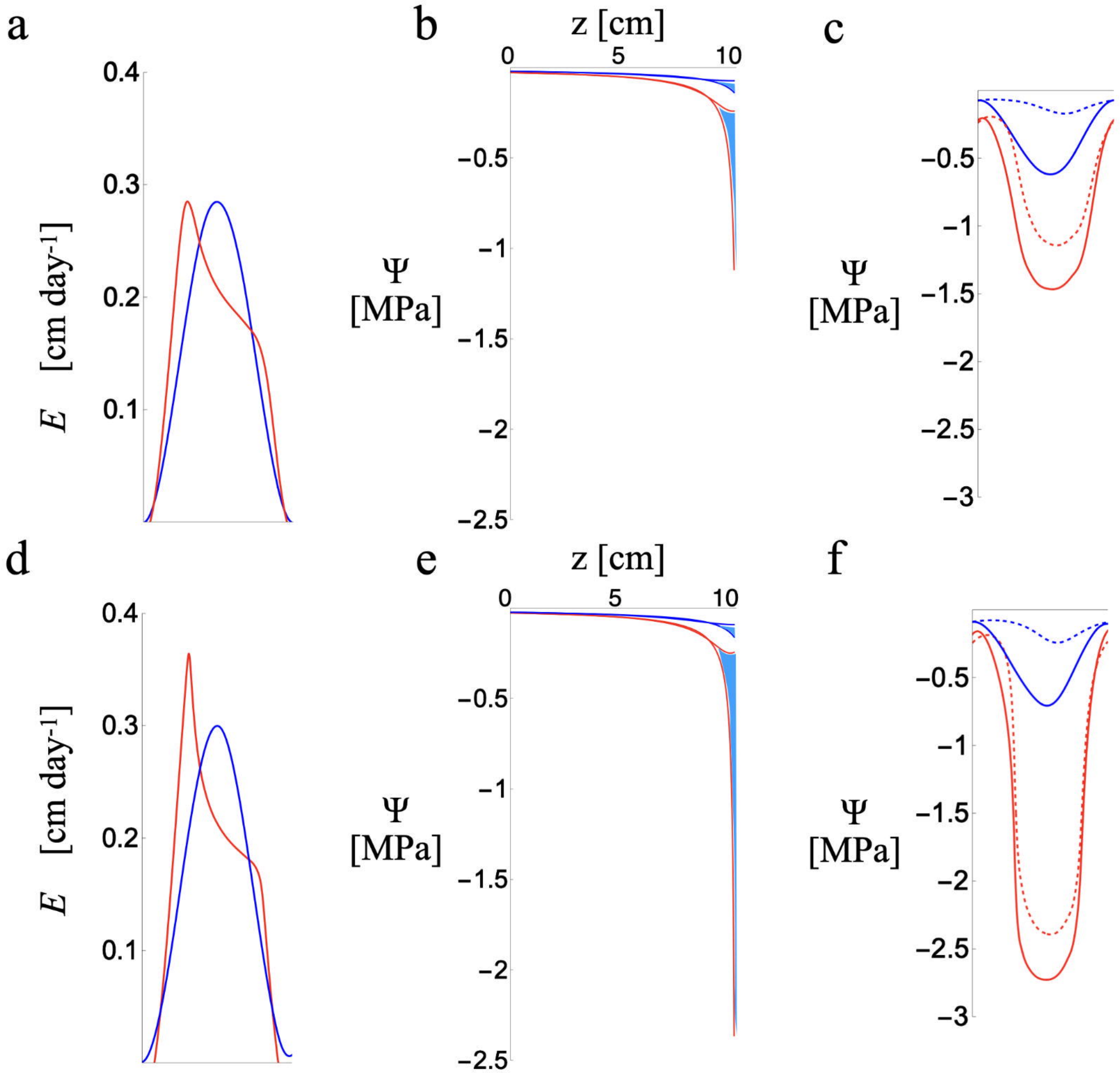

Figure **4**. Effect of doubling $g_s\Psi 50$ ('osmotic adjustment') from -1.33 MPa (**a**,**b**,**c**) to -2.66 MPa (**d**,**e**,**f**) with *nVPD* 1 (blue) and *nVPD* 2 (red). **a,d** Diel course of transpiration in the stationary state: maintaining higher g_s to lower Ψ stretches the a.m. peak, but E for both setpoints converges rapidly once stomata start to constrain the water flux. **b**,**e** Gradients of water potential through the soil domain at the nocturnal maximum and diurnal minimum of *nVPD*: the space between the two lines (light blue) for each level of *nVPD* shows the region of the domain subject to daily fluctuations in water content, which remain confined to near the rooting plane (z=10 cm). **c**,**f** Diel course of soil (dashed) and leaf (solid) water potential; at *nVPD* 2 shifting stomatal closure to a value twice as negative allows leaf water potential to fall to values almost twice as dry but fails to pull a larger midday or total daily water flux from the soil (**a**,**d**).

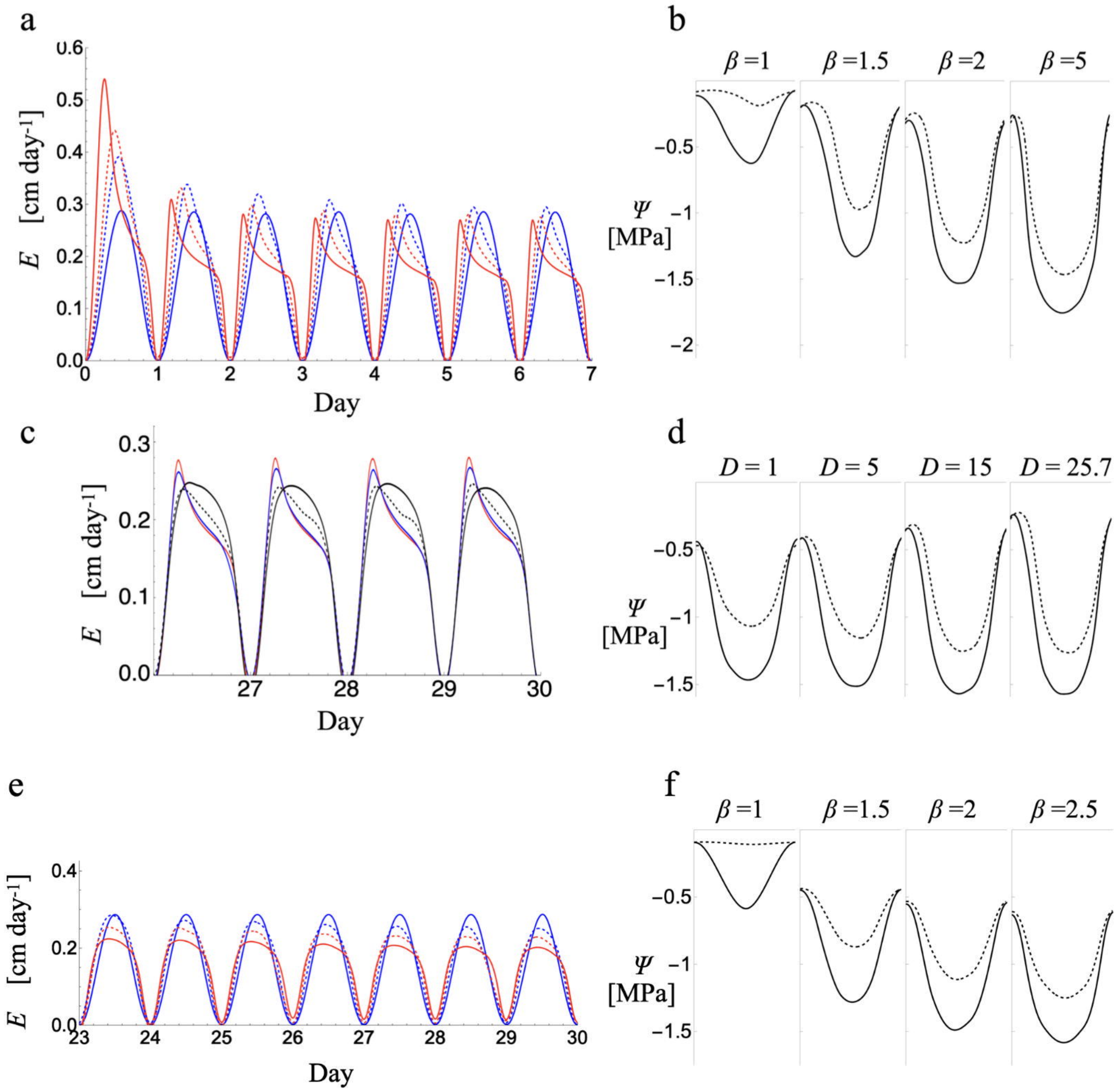

Figure **5.** Emergence of feedforward behavior and isohydry from different aspects of the soil plant system. **a** Parametric sweep across β levels 1 (blue solid), 1.5 (blue dashed), 2 (red dashed) and 5 (red solid) showing the emergence of feedforward behavior at D_o=25.7. **b** Diel course of leaf (solid) and root (dashed) water potentials showing the transition from anisohydric to isohydric for the same simulations as in **a**. **c** Decay of feedforward behavior at β=2.5 as D_o falls from 25.7 (red) to 15 (blue), 5 (black dashed) and 1 (black solid). **d** Diel course of leaf (solid) and root (dashed) water potentials for the simulations in **c** showing no change in the pattern of midday leaf water potentials but greater relaxation at pre-dawn as D_o falls. **e** Parametric sweep across β levels 1 (blue solid), 1.5 (blue dashed), 2 (red dashed) and 2.5 (red solid) showing peak broadening replaces the emergence of feedforward behavior from increasing supply and demand imbalance at D_o=1. **f** The emergence of isohydry at D_o=1 follows the same pattern as at D_o=25.7.

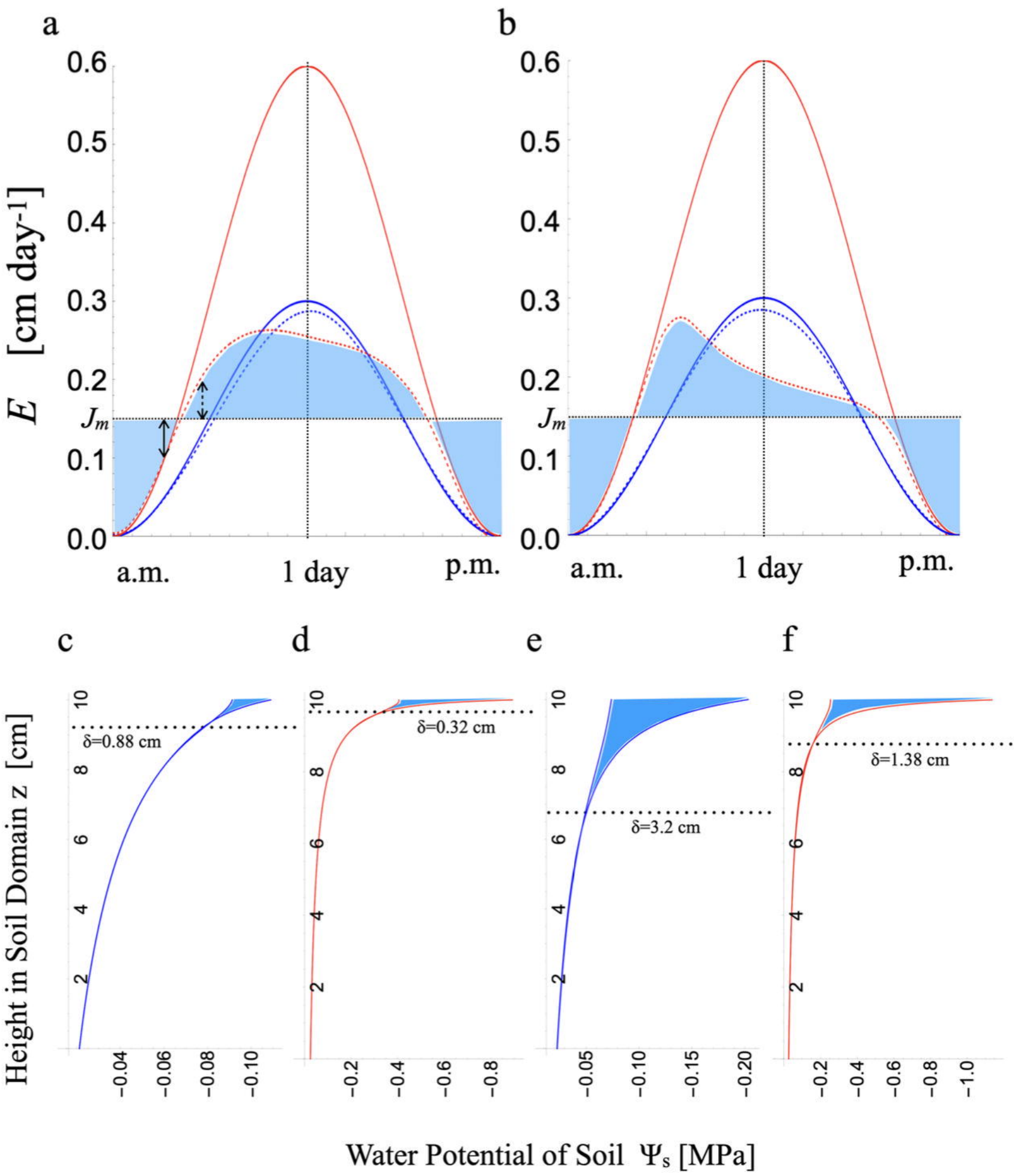

Figure **6**. Diel course of potential transpiration (solid) and actual transpiration E (dashed) in the stationary state at β=1 (blue) and β =2 (red), for a soil diffusivity set to 1 cm^2 s^{-1} (**a**) and 25.7 cm^2 s^{-1} (**b**); light blue shading indicates periods of net recharge (below the steady inward soil flux J_m) and discharge (above J_m) of the 10 cm deep model domain with respect to the β=2 case, with the heights (solid and dashed arrows respectively) proportional to the magnitude of the recharge/discharge flux at that instant. Note the total areas under all the dashed lines are approximately equal. **c,d,e,f**: Gradients in water potential through the soil domain to the root plane at z=10 at the daily minimum and maximums of E; the intervening space (light blue) shows the region and potential range for transient release of water over this period (note the difference in potential scales), relative to the damping depth δ, which represents how far into the soil domain diel variations are expected to reach. Panels **c,d** correspond to **a,** and **e,f** to **b.** Note that differences in areas between the gradients (light blue) across **c,d,e,f** cannot be simply interpreted as differences in the volumes of water released due to differences in scale.

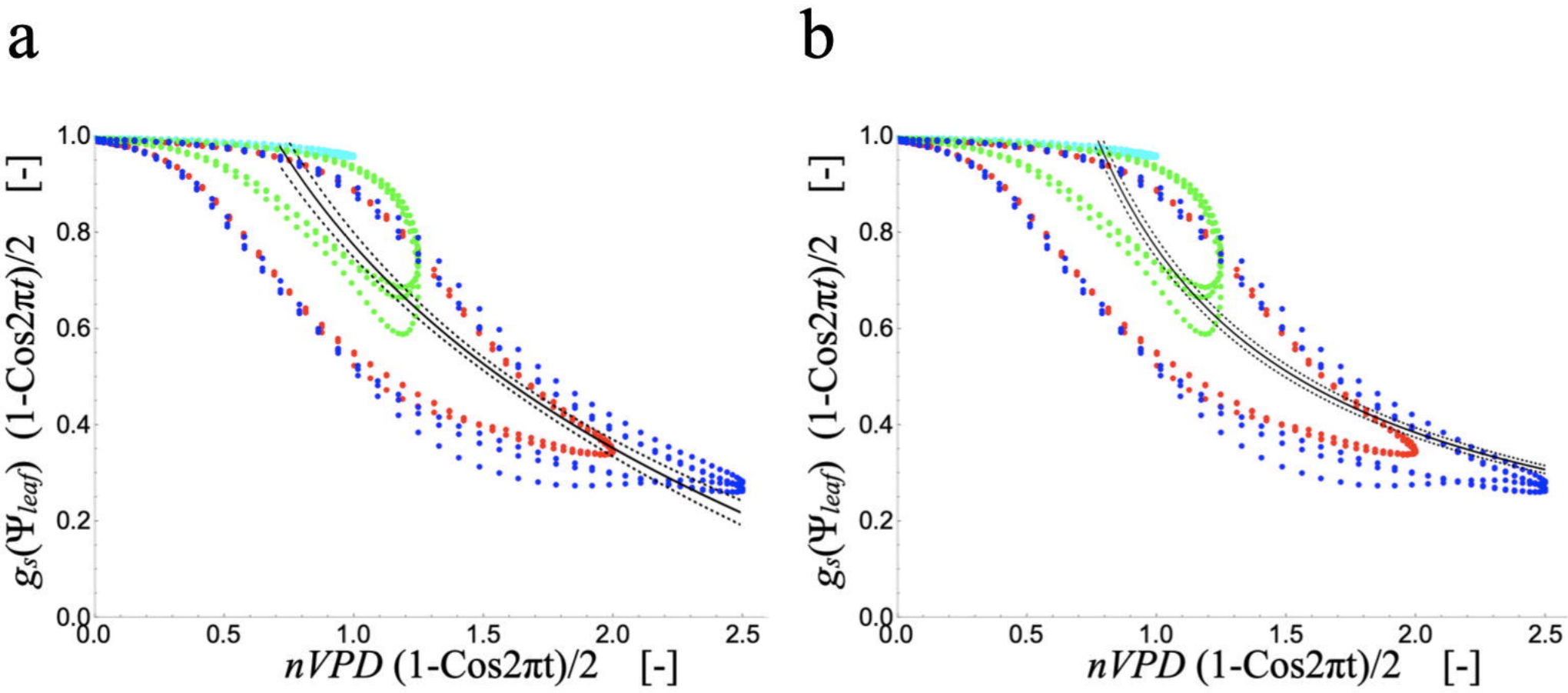

Figure **7**. Fits of simulated diurnal values (hysteretic loops) of stomatal conductance for two contrasting models of stomatal sensitivity to *VPD*. Data are for all four modeled *nVPD* levels (cyan 1, green 1.25, red 2, blue 2.5); black solid lines show the fit and dashed lines the 99% CI. **a** Log-based model: $g_s = g_{s,ref}(1 - m \ln[nVPD])$, $g_{s,ref} = 0.78$, $m = 0.79$, adj$R^2 = 0.96$. **b** Mass-balance based model: $g_s = g_{s,ref}/nVPD$, $g_{s,ref} = 0.78$, adj$R^2 = 0.96$.

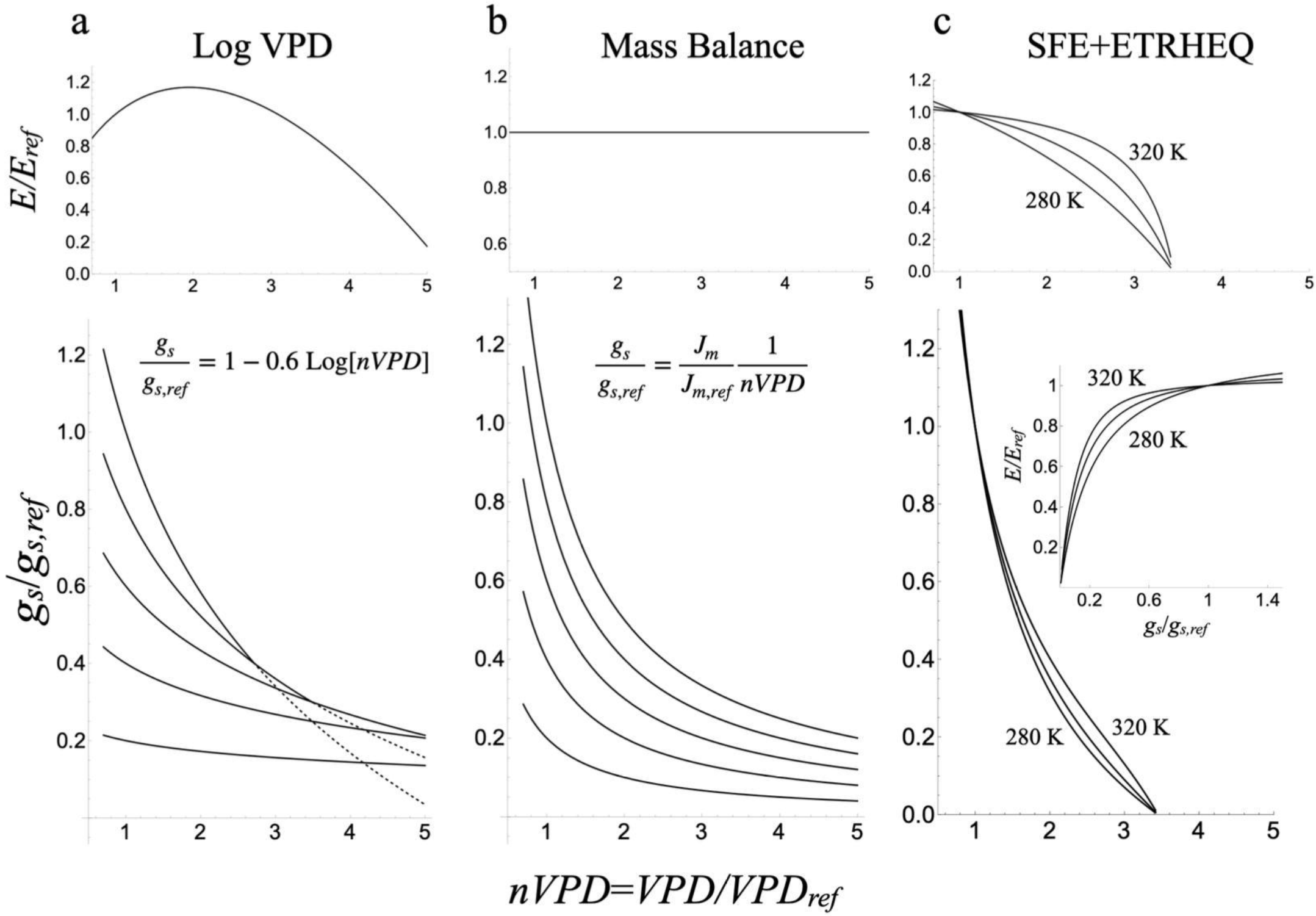

Figure **8**. A comparison of the normalized conductance extinction curves ($g_s/g_{s,ref}$) and transpiration responses (E/E_{ref}) for three simplified models of stomatal responses to soil drying and atmospheric aridity, with 1 kPa as the reference state for *nVPD*. **a** Based on the behavior of the dry sites in figure 2 of Novick *et al.* (2016), as the soil dries in the model $g_s/g_{s,ref} = a\ (1 - m \ln[nVPD])$ the intercept a falls from 1 at $nVPD = 1$ to 0.2 while the slope m falls from 0.6 to 0.2. Note that the curves representing *nVPD* responses at higher soil moisture are predicted to cross (at the transition from solid to dashed) the curves for lower soil moisture. **b** For the mass balance model $g_s/g_{s,ref} = (J_m/J_{m,ref})\ (1/nVPD)$, $J_m/J_{m,ref}$ falls from 1 to 0.2 to simulate a falling maximum flux as the soil dries. **c** Under the condition of Surface Flux Equilibrium (SFE), the atmospheric boundary layer approaches a constant RH (and potential *nVPD*) at all heights; responses are shown for air temperatures at two meters above the canopy of 280, 300 and 320 K.